Collagen matrices: biomaterials for selective cell response

by

©Zhe Dong

A Dissertation submitted to the School of Graduate Studies in partial fulfillment of the requirements for the degree of

M.Sc.

Department of Chemistry

Memorial University of Newfoundland

September 2017

St. John's Newfoundland

Abstract

This thesis covers two types of biomaterials: collagen matrices for cell culture and segmental-long-spacing (SLS) collagen. They are both based on type I collagen, yet have distinct configurations.

Cells are supported by extracellular matrix (ECM) proteins which can actively influence differentiation, growth, and function of cells. We used type-I collagen, which is the most abundant fibrous protein in the ECM, to establish a model physical context for cell-cell interaction suitable to study the impacts of fat cells (adipocytes) on breast cancer cells. This model system incorporates interactions with the collagen matrix to selectively manipulate adipocyte development or function as defined by triglyceride accumulation as well as leptin and adiponectin secretion. The morphology and elasticity of collagen matrices in the presence and absence of adipocytes, as measured by atomic force microscopy (AFM), indicates that adipocytes altered collagen elasticity in a manner dependent both on adipocyte developmental stage and the collagen preparation.

Overall, it is feasible to selectively manipulate the physiology and functionality of adipocytes by timing the addition of specific collagen overlays in combination with specific tissue-culture plates. These findings have implications for analysis of adipocyte development *in vitro* as well as potential therapeutic implications to specifically alter adipocyte functionality, which is reported to have impacts on regulating

the proliferation of breast cancer cells.

As to the SLS collagen, we prepared the samples in different pH environments to seek the influence of pH on the formation of SLS collagen. The result reveals that the less acidic environment (pH=4) favours the formation of long fibers, which is more similar to the native-type configuration of type I collagen aggregation. On the contrary, in the more acidic environment (pH=2), the individual block-like SLS collagen is the major product. Yet, the specific mechanism of the synthesis of SLS collagen still requires more investigation. This work provides the basis for further study to synthesize SLS collagen with tunable length, thickness, and/or surface banding distance, with various applications such as matrices for the cell culture.

Acknowledgements

First and foremost, I would like to thank Dr. Erika Merschrod, my supervisor, who gave me the opportunity to conduct research in her group. I appreciate all the great inspiration, encouragement, and support from her. It has been so many times that her wisdom helps me get rid of my frustrations. I would not have finished my program without her help.

Then I would also like to thank Dr. Sherri Christian and her student Nikitha Kendyala. They completed the delicate sample preparation and assisted with the interpretation of biochemistry data.

Also a big thank you to all the Merschrod group members. I really enjoy our weekly group meeting, where we can all give and receive help from each other.

Last but not least, thanks to Memorial University, especially the Department of Chemistry, who offered me a great place to live and study. Thanks to all the funding resources: NSERC, SGS, and CFI.

Table of Contents

List of Figures

List of Abbreviations and Symbols

AFM	Atomic Force Microscopy
ATP	adenosine-5'-triphosphate
BAT	Brown Adipose Tissue
C/EBP-α	CCAAT/enhancer-binding protein alpha
d	the deflection of the cantilever of the AFM tip
Δd	the jump to contact distance
δ	the tip-sample separation distance
E_s	Young's Modulus
ECM	Extracellular Matrix
EFM	Electrostatic Force Microscopy
EHS	Engelbreth-Holm-Swarm
F	the applied force
F_p	adhesive force
$\|F_p\|$	the jump off contact force
FFA	Free Fatty Acids
FS	Force Spectroscopy

JKR	Johnson-Kendall-Roberts
k	the spring constant of the cantilever
LFM	Lateral Force Microscopy
MFM	Magnetic Force Microscopy
ν_s	the Poisson's ratio
PBS	Phosphate Buffered Saline
pI	isoelectric point
PPAR-γ	peroxisome proliferator-activated receptor gamma
R	the radius of the AFM tip
Sem	Standard error of mean
SLS	Segmental Long Spacing
SPM	Scanning Probe Microscopy
TG	Triglycerides
WAT	White Adipose Tissue

Chapter 1

Introduction

1.1 Adipocytes

1.1.1 Obesity increases the rates of breast cancer

Obesity rates have been doubling globally since 2008, with an estimated 13% of adults being obese in 2015 [1]. In Canada, specifically in Newfoundland and Labrador, a recent survey shows that approximately 34% of adults are obese [2]. Being obese is correlated with increased rates of various diseases, including cardiovascular disease, Type 2 diabetes, and breast cancer, with a burden of disease that is higher than with smoking [3]. Considering the serious consequences of obesity, it is essential to put much more effort into investigating, and then ideally controlling obesity, which is essentially the pathological enlargement of adipose tissue [4]. Hence, to have a better understanding, some basic information about adipose tissue will be introduced in this chapter.

1.1.2 The comparison between brown and white adipose tissue

In mammals, two major types of adipose tissue have been identified: brown adipose tissue (BAT), and white adipose tissue (WAT). [5]

From the aspect of appearance, the BAT [6] has a large amount of mitochondria that contribute to producing energy and contain iron cations, [7] which gives the brown color to the tissue. In addition, there are usually multiple small lipid droplets accumulated in brown fat cell; however, in a white fat cell [8] only one giant lipid droplet is present and occupies the whole cell.

From the aspect of function, the BAT [6] can generate heat in a non-shivering way. This explains why the BAT mainly exists in newborns [9], who can only generate heat by non-shivering means. Hence the level of the BAT content decreases when mammals grow up and gain the ability to shiver to produce heat [10]. The WAT [8] has relatively more functions including being a cushion to protect organs, a thermal insulator, and to maintain the energy homeostasis in our body, which involves the formation of triglycerides (TG) from free fatty acids (FFA). The total amount of TG stored in WAT is proportional to both the size and number of adipocytes, which are the major component of WAT.

Mature, TG-laden adipocytes develop from fate-committed pre-adipocytes through the activation of a series of well-regulated transcription factors culminating in the increased expression of C/EBP-α (a type of transcription factor) and PPAR-γ (a type of nuclear receptor), often termed the "master regulators" of adipogenesis [11]. Increased expression of C/EBP-α and PPAR-γ promote expression of key proteins essential for lipid and carbohydrate storage proteins, such as Glut4 and perilipin, allowing formation of large lipid droplets, the main feature that characterizes terminal differentiation

into mature adipocytes [12]. In addition, the newest discovered function of WAT, as well as what draws our attention to study adipocytes, is its ability to signal to other tissues as an endocrine organ through adipokines [13].

1.1.3 Adipokines: the signaling proteins

In 1994, an unique protein, leptin, was discovered and proved to be able to regulate the body weight of rodents [14]. This finding gave WAT another major role of being an endocrine organ, rather than a simple energy reservoir. In the following couple of years, more and more similar signaling proteins produced by WAT were discovered; to date, hundreds have been identified and named "adipokines", e.g. leptin, adiponectin, and tumor necrosis factor-alpha [15]. Herein, I will mainly focus on discussing leptin and adiponectin due to their distinct impacts on regulating the proliferation of breast cancer cells.

As mentioned earlier, leptin can help regulate body weight by inhibiting the appetite [16]. Hence the secretion of leptin is elevated in obese individuals and decreased with fasting. In contrast, adiponectin is inversely associated with obesity and increases with fasting [17]. Both adiponectin and leptin are secreted from terminally differentiated adipocytes and act on WAT as well as distal tissues. For example, adiponectin enhances insulin sensitivity and induces expansion of WAT, which prevents the toxic deposition of free fatty acids in other organs [18], whereas leptin acts through the sympathetic nervous system to induce lypolysis of WAT [19]. In contrast, both adiponectin and leptin can promote glucose uptake by skeletal muscle [20].

Interestingly, both leptin and adiponectin have also been shown to directly regulate cancer cell proliferation. Leptin promotes proliferation of breast cancer cells [21], while adiponectin inhibits their proliferation [22]. Thus, adipokines secreted by WAT have multiple and varied effects on select tissues and cells. This brings up the urgent

need of establishing a three-dimensional (3D) co-culture system, where adipocytes can be cultured together with the target cells (the breast cancer cells in our system) to specifically study the signaling interactions.

1.2 The 3D co-culture system

Essentially, we are building a system as shown in Figure 1.1, in which the adipocytes are placed as the bottom layer, and the breast cancer cells are cultured as the top layer. The two layers of cells are separated by an artificial extracellular matrix (ECM), which works as a physical barrier but meanwhile also allows the unrestricted traversing of signaling molecules.

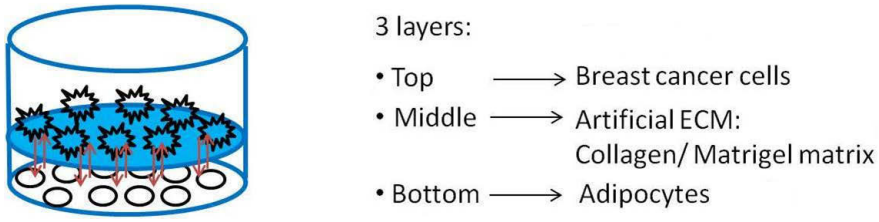

Figure 1.1: The schematic of our 3D co-culture system with adipocytes, breast cancer cells, and the artificial extracellular matrix (ECM)

The middle artificial ECM layer acts as a scaffold, as well as providing the micro-environment to cells. To mimic *in vitro* the physiological state of the ECM *in vivo*, which contains the interstitial matrix and the basement membrane [23], I adopted native type I collagen and Matrigel matrix (Section 1.2.2) in the artificial ECM layer. In the next section, I will introduce some background information regarding the ECM.

1.2.1 Extracellular matrix (ECM) *in vivo*

In animals, ECM is the physiological living environment for cells [24]. Other than physically supporting cells, it produces a range of biochemical cues that can regulate

cell behaviours, including cell adhesion, proliferation, and differentiation [24].

As the major component of ECM, the interstitial matrix mainly consists of polysaccharides and fibrous proteins (mostly fibrillar collagen) [25]. The high fibrillar collagen content determines the fibrous structure of the interstitial matrix. However, the other component basement membrane, which serves as the physical barrier between epithelial cells and the adjacent interstitial matrix, has a distinct sheet-like network [26]. This is due to the high level of type IV collagen, which is a type of non-fibrillar collagen mainly in the basement membrane [27].

The specific constitution of ECM varies among different organs, but in adipose tissue the major proteins include types I, IV and V collagen and fibronectin, as shown in Figure 1.2 [28]. Among all the proteins, type I collagen is functionally and structurally the major one; the other proteins work together to associate type I collagen fibers with the adipocyte.

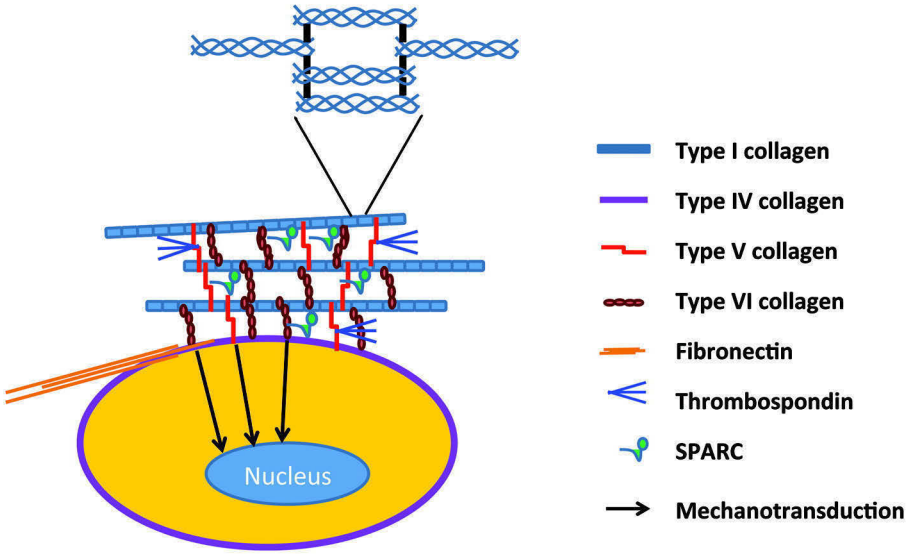

Figure 1.2: The schematic shows the major protein composition in adipose tissue [28] The cell in the schematic is and adipocyte. In addition to various types of collagen, other proteins are also present, such as fibronectin, thrombospondin and SPARC.

Again, in our system, I used native type I collagen, the most abundant collagen,

as the representative of interstitial matrix. I adopted Matrigel, an extraction from mouse tumor cells [29], to mimic the basement membrane.

1.2.2 Matrigel

Matrigel is a commercialized protein complex that is extracted from the ECM of Engelbreth-Holm-Swarm (EHS) mouse tumor cells [29]. To date, the specific constitution of Matrigel still remains unknown. The primary proteins that have been identified in Matrigel include type IV collagen, laminin, enactin, and various growth factors [30], which are all the major components of basement membrane. Thus, Matrigel has been widely used as the reconstituted basement membrane [31].

Matrigel has been used as the optimal matrix for many cell cultures, especially stem cells, for decades. This is mainly due to its ability to hold the stem cells in an undifferentiated state for different study purposes, even though the underlying mechanism also remains unclear [30]. In addition, cancer cell studies also commonly adopt Matrigel as the matrix, as it is an extraction from tumor cells [32].

Despite all the popularity of using Matrigel as the cell culture matrix, I decided to start with native type I collagen matrix, which is better understood and also commonly used in cell culture [33], as the starting point of the co-culture system.

1.2.3 Native type I collagen

Collagen is a fascinating type of protein that exists in most animals' organs and tissues, including tendon, skin, teeth and cartilage [34]. As the most abundant protein in mammals, the major role of collagen is as a structural protein, especially in connective tissue [35].

To date, 28 types of collagen have been identified [36]. According to their configurations, which are decided by the primary amino acid sequence, they are separated

into two groups: fibrillar collagen and non-fibrillar collagen [37]. Among fibrillar collagen, the most common one is type I collagen, which takes up almost 90% of all collagen in our body [38]. Similar to the other fibrillar collagen, type I collagen has a hierarchical structure [39], as explained in Figure 1.3. Three left-handed helical chains twist together to form a right-handed collagen monomer; then monomers aggregate to form a collagen micro-fibril. Further on, micro-fibrils line up to fibrils, then to form long fibers. Eventually, the fibers assemble to form bulky tissues and organs. One unique character of collagen fibers, as indicated in Figure 1.3, is the surface banding. According to literature, the specific distance between the adjacent bandings on type I collagen fibers is 67 nm [40]. This character can be used as the criteria to identify type I among all the fibrillar collagens.

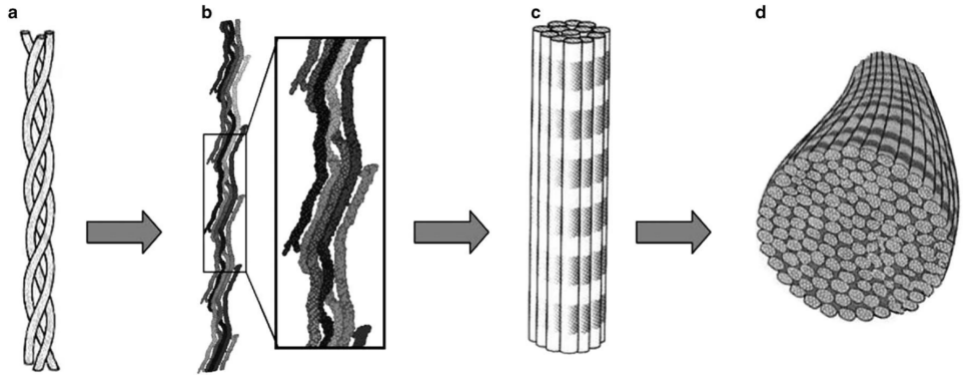

Figure 1.3: The schematic shows the hierarchical structure of fibrillar collagen. a: collagen monomer; b: micro-fibril; c: fibril; d: fiber [39]

Figure 1.4 is the atomic force microscopy (AFM) deflection image I collected of one of the type I collagen matrices. According to the section analysis (data not shown), the distance between two adjacent bandings is uniformly 67 nm. This finding confirmed that the collagen matrices were successfully prepared without substantially altering the morphological character (surface banding) of collagen fibers.

Type I collagen matrix has been widely adopted as a cell culture matrix [41], due to its abundance in physiological ECM. Hence, I altered native type I collagen into

into two groups: fibrillar collagen and non-fibrillar collagen [37]. Among fibrillar collagen, the most common one is type I collagen, which takes up almost 90% of all collagen in our body [38]. Similar to the other fibrillar collagen, type I collagen has a hierarchical structure [39], as explained in Figure 1.3. Three left-handed helical chains twist together to form a right-handed collagen monomer; then monomers aggregate to form a collagen micro-fibril. Further on, micro-fibrils line up to fibrils, then to form long fibers. Eventually, the fibers assemble to form bulky tissues and organs. One unique character of collagen fibers, as indicated in Figure 1.3, is the surface banding. According to literature, the specific distance between the adjacent bandings on type I collagen fibers is 67 nm [40]. This character can be used as the criteria to identify type I among all the fibrillar collagens.

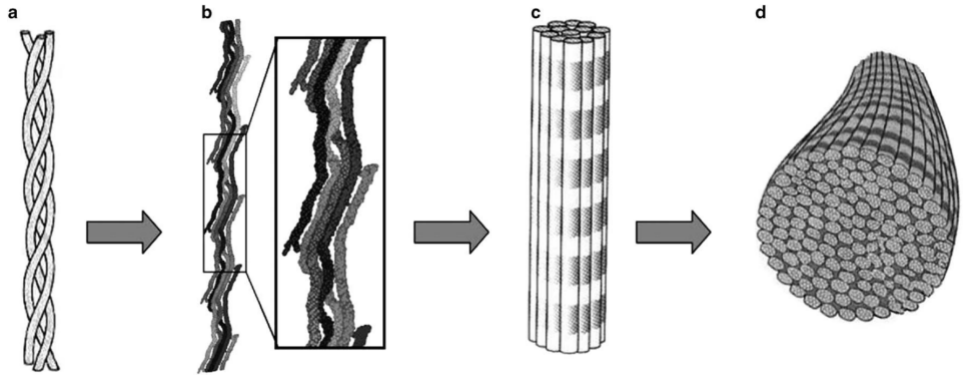

Figure 1.3: The schematic shows the hierarchical structure of fibrillar collagen. a: collagen monomer; b: micro-fibril; c: fibril; d: fiber [39]

Figure 1.4 is the atomic force microscopy (AFM) deflection image I collected of one of the type I collagen matrices. According to the section analysis (data not shown), the distance between two adjacent bandings is uniformly 67 nm. This finding confirmed that the collagen matrices were successfully prepared without substantially altering the morphological character (surface banding) of collagen fibers.

Type I collagen matrix has been widely adopted as a cell culture matrix [41], due to its abundance in physiological ECM. Hence, I altered native type I collagen into

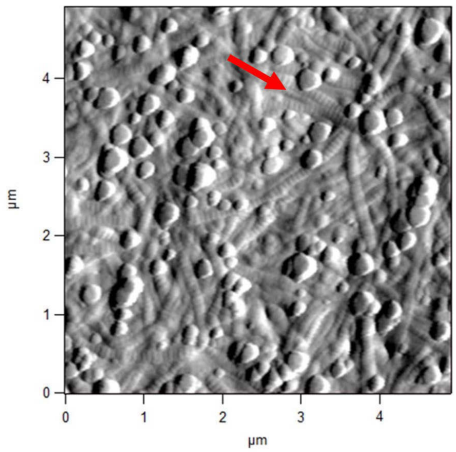

Figure 1.4: The AFM deflection image of type I collagen matrix shows the characteristic 67 nm surface banding. The arrow indicates the surface banding

matrices by two different preparations to study the interactions between collagen and adipocytes, and seek the influence on adipogenesis from different matrices preparation methods.

1.3 Segmental-long-space (SLS) collagen

Another collagen-based biomaterial I studied was segmental-long-spacing (SLS) collagen. Even though, as introduced previously, native type I collagen is the most abundant fibrillar collagen, another configuration of type I collagen aggregate exists *in vivo* i.e. SLS collagen. As shown in Figure 1.5, SLS collagen aggregates have a block-like structure. The length of the SLS block is approximately 280 nm, which is the same as a collagen monomer [42]. Hence, SLS collagen has been used as a system to study the properties of the collagen monomer, which is usually difficult to study due to its small size, since SLS is essentially collagen monomers assembling in register and then amplifying the physical properties [43].

The existence of SLS collagen *in vivo* was firstly reported in 1979 [44]. Collagen monomers aggregate to form SLS collagen blocks to avoid being attacked by enzymes

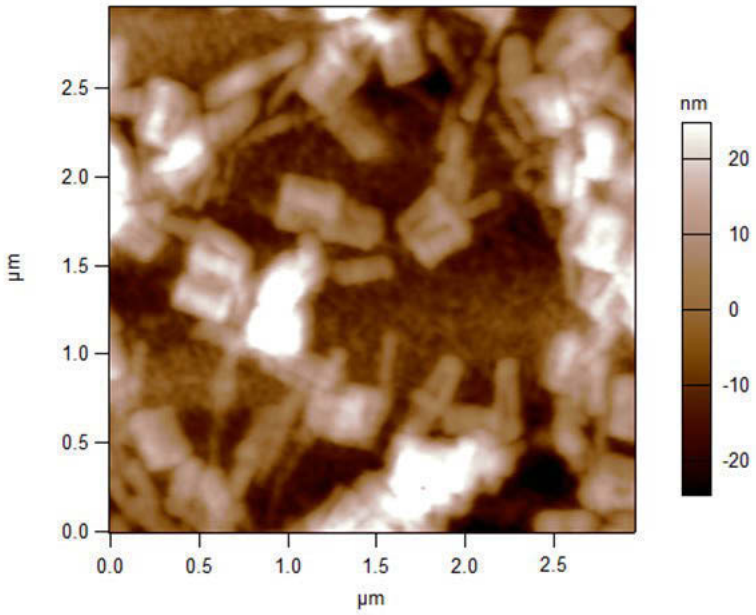

Figure 1.5: AFM image of SLS collagen shows the special block-like structure

during collagen transport [44].

SLS collagen can be easily reproduced *in vitro* by the addition of adenosine-5'-triphosphate (ATP) into collagen monomer solution, within a certain range of pH values [44]. However, the specific role of ATP molecules and the mechanism of SLS collagen formation still remain unclear. In my project, I adjusted the pH value of the collagen solution to seek the influence of pH on SLS collagen formation.

1.4 Atomic force microscopy

Atomic force microscopy (AFM) is a type of scanning probe microscopy (SPM) with very high resolution. In comparison to the conventional optical microscopy, whose resolution is limited by the optical diffraction limit [45], AFM records the morphology of samples by physically scanning across the sample surface using a tiny tip [46]. Hence, under ideal experimental conditions (vacuum, sharp tip, etc.) the spatial

resolution can reach the atomic level [47]. Other than high resolution, AFM also possesses many other advantages. For example, it does not require much complicated sample preparations, nor does it damage the sample [48]. In addition, the ability of performing measurements in solution makes AFM the perfect technique in multiple fields especially in biology and chemistry [49].

AFM has many practical applications including lateral force microscopy (LFM), magnetic force microscopy (MFM), electrostatic force microscopy (EFM), and force spectroscopy (FS) [50]. In my project, I used force spectroscopy to measure the elasticity (defined by Young's Modulus) of the matrices, with and without the presence of adipocytes. In addition, FS can also provide information regarding the visco-elasticity of the sample [51], which is a valuable property to investigate in biological tissues.

1.4.1 The mechanism of AFM

Even though AFM can measure a wide range of properties on many different types of samples, the mechanism of its operation is relatively simple. As shown in Figure 1.6, a laser beam is shone on the back of an AFM cantilever. During the scanning, the tip moves up and down according to the surface features it may encounter. Then the change of tip movement will be monitored by the detector and adjusted by the feedback loop, to maintain a user-defined distance between tip and sample. Eventually the system give a high resolution AFM image that consists of many tiny pixels, which were combined together to rebuild the surface features of the sample.

1.4.2 Contact mode

Mainly, AFM has two working modes: contact mode and tapping mode. Contact mode is easier to operate; however, tapping mode can better protect the sample from

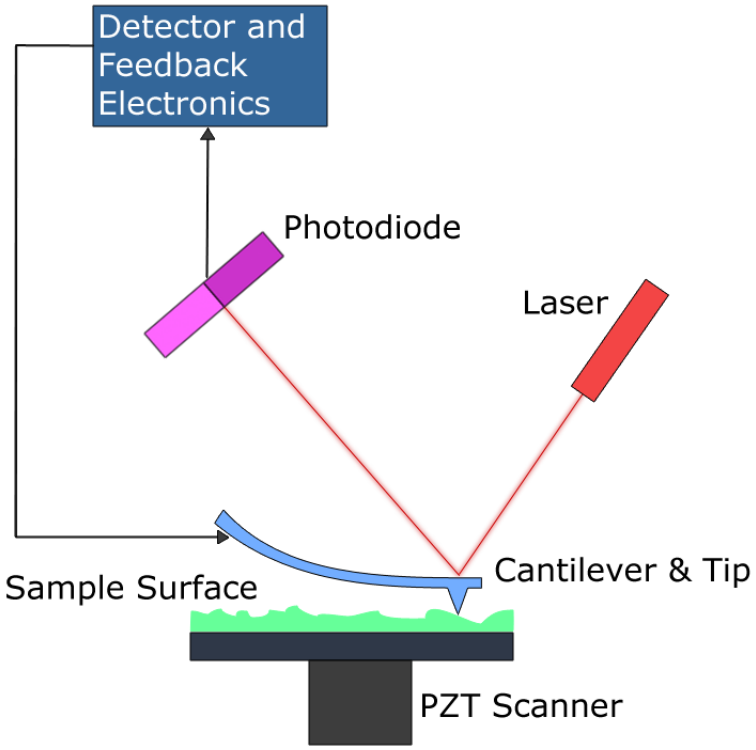

Figure 1.6: The schematic of the AFM setup. By Askewmind [Public domain], via Wikimedia Commons

being damaged. In my project, most of the study was done under contact mode.

In contact mode, the AFM tip keeps in contact with the sample surface during scanning. So once the tip meets higher or lower features, the cantilever will correspondingly bend against or towards the sample to make sure the tip and sample are in contact. This bending causes a variation in deflection of the laser. Then a feedback loop adjusts the deflection back to a pre-defined "setpoint". In tapping mode, however, instead of remaining in contact with sample, the AFM tip keeps tapping on the sample surface with a set amplitude and frequency. The surface features cause a change of tapping amplitude, which is recorded and adjusted back to the setpoint by the feedback loop. [48]

1.4.3 Force spectroscopy

Force spectroscopy is a practical application of AFM. It can accurately assess the mechanical properties of a sample at difference length scales, depends on the geometry of the chosen tips. The scale of the applied and measured forces can be as small as piconewtons [52]. Force spectroscopy uses the AFM tip as an indentor. By applying force on the tip, the tip will indent into the samples for a certain indentation depth that depends on the mechanics of the sample [53].

During the indentation, the deflection of the cantilever (d) and the tip-sample separation distance (δ) are monitored and recorded. Accurate measurements require instrument calibration before the experiment. The calibration [54] is to conduct an indentation on a rigid, non-compressible surface (e.g. silicon wafer or mica), on which the tip cannot make an indentation. Hence the tip-sample separation δ is 0. Then the vertical displacement completely results from the deflection of cantilever. The applied force can accurately be correlated with the deflection by Hooke's law:

$$F = -kd \tag{1.1}$$

where F is the applied force, d is the deflection of the cantilever, and k is the spring constant of the cantilever, which can be determined by the thermal noise method [55].

Each indentation generates a deflection-displacement curve, or force curve, as in Figure 1.7, which can be easily converted into force-distance curve as in Figure 1.8.

The red curve in Figure 1.7 corresponds to the tip approaching the sample. With the distance between tip and sample getting smaller, the van der Waals attractive force is getting stronger. When they get close enough, the tip will suddenly land on the sample, which causes the abrupt decrease in deflection. Then the oblique segment is the indentation phase. The retract (blue line) starts when the indentation

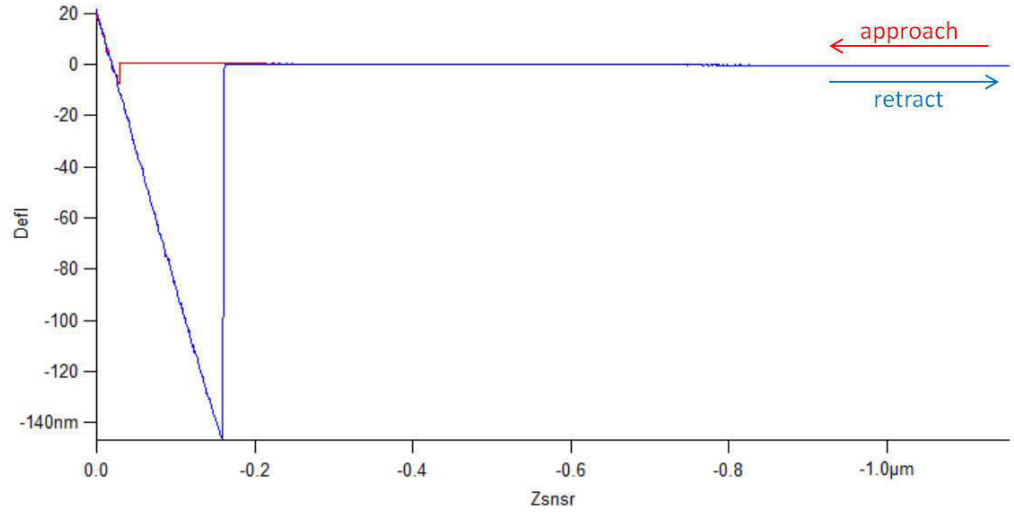

Figure 1.7: AFM indentation deflection-displacement curve

force reaches the user defined "trigger point". The oblique segment on the blue curve represents the retraction. However, the van der Waals adhesion force between tip and sample holds the tip from immediately pulling from the sample. The system will keep applying a retracting force until it can balance the adhesion force; then the tip will jump away from surface, which gives the vertical segment on the blue curve.

Other than conducting an individual force curve at a single point, there is another method, i.e. force mapping, to easily investigate the mechanical properties of an overall area on the sample surface. A regular AFM scan generates an image that reflects the morphology of sample as in Figure 1.9 left. We can perform force mapping on the same area with a user-defined resolution (16×16 pixels in Figure 1.9 right), where each pixel represents an individual force curve. Then mechanical parameters such as Young's Modulus can be calculated from each curve, with an average used to assess the overall elasticity of the scanned area.

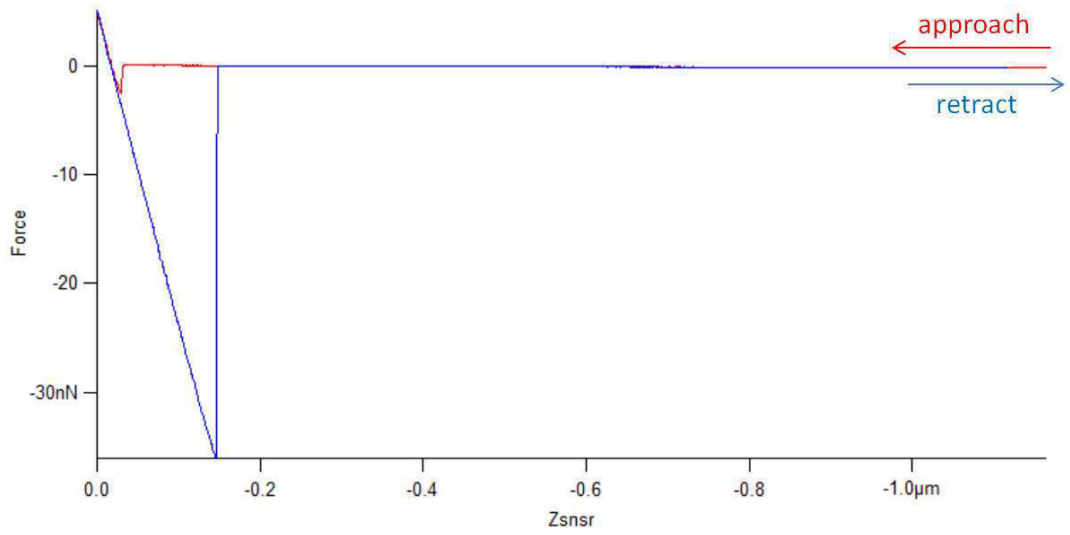

Figure 1.8: AFM indentation force-displacement curve

1.4.4 Minimum nano-indentation

Nano-indentation of AFM force spectroscopy can largely protect the sample from being destroyed. It still has great interest to come up with a method that can indent to a minimum depth but still guarantee a meaningful measurement. Chuan Xu, a former PhD student in our group, developed the minimum nano-indentation method to investigate the mechanics of soft tissues [56]. In this method, Dr. Xu minimized the trigger point down to 5 nN, which causes an indentation depth of less than 10 nm with the samples and tips from this project.

Conventionally, the force curve can be fitted with mathematical models like the Hertzian model [57] or the Johnson-Kendall-Roberts (JKR) model [58], depending on the geometry of the tip and the scale of the adhesion force. The Hertzian model fitting requires a spherical AFM tip and a flat sample surface, and no adhesion between tip and sample. Hence, the Hertzian model is more suitable in the mechanics study in aqueous environment, where the adhesive force is eliminated by water [59]. However, in my project, most of the samples were investigated in air, where the samples were

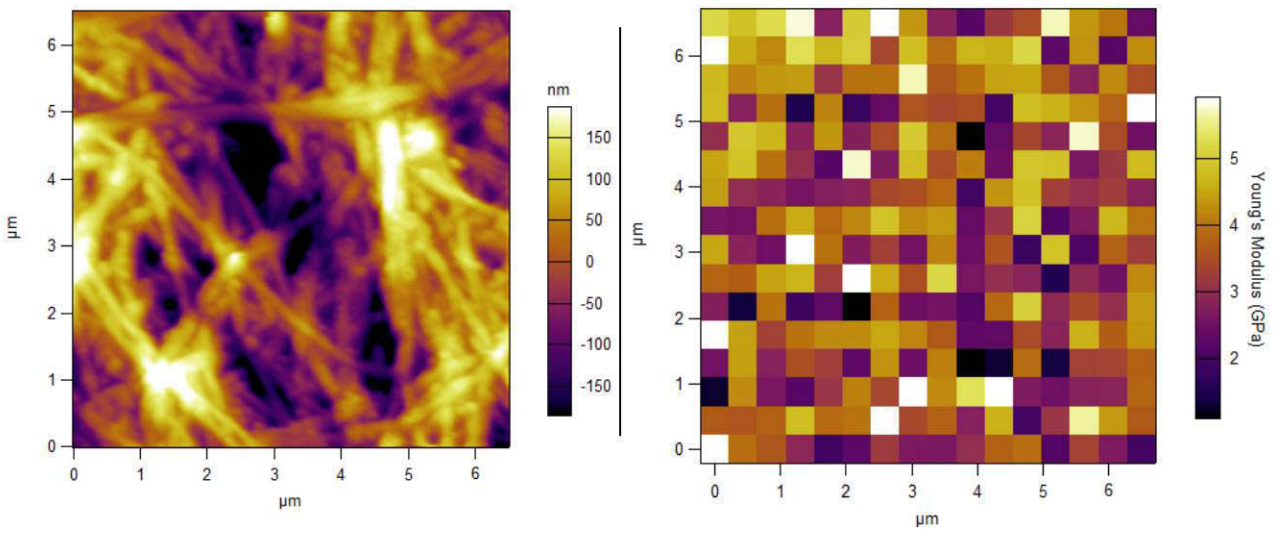

Figure 1.9: Left: AFM height image of collagen matrix; Right: the 16×16 pixel force map of the same area as the height image.

directly exposed in air instead of being soaked in solutions, so the tip-sample adhesion exists and is significant enough (as in Figure 1.7) that it cannot be neglected. Thus, the JKR model, which takes the adhesion between tip and sample into account, is a better model in my study.

The JKR model offers the following equation to fit with the AFM force curves:

$$E_s = \frac{-3F_p}{\sqrt{R}}(1-\nu_s^2)\left[\frac{3(\delta_0-\delta_{adh})}{1+4^{-\frac{2}{3}}}\right]^{-\frac{3}{2}} \tag{1.2}$$

where, E_s is the Young's Modulus of the sample, F_p is the adhesive force between tip and sample, R is the radius of tip, and ν_s is the Poisson's ratio of the sample (biological samples usually are assumed to have $\nu_s = 0.5$ [54]). δ_0 and δ_{adh} are the tip displacements when the applied force is zero and when it balances the maximum adhesive force, respectively.

To closely fit the force curve obtained by the minimum nano-indentation method,

Xu modified the JKR equation to the following format:

$$E_s = \frac{5}{2}|F_p|R^{-\frac{1}{2}}(1-\nu_s^2)\left(\Delta d - 2\left(\frac{AR}{24k}\right)^{\frac{1}{3}}\right)^{-\frac{3}{2}} \tag{1.3}$$

Different from Equation 1.2, Δd and $|F_p|$ are the jump to contact distance (the abrupt decrease on the red curve in Figure 1.7) and the jump off contact force (the abrupt decrease on the blue curve in Figure 1.8), and A is the Hamaker constant that can be calculated through the following equation [60]:

$$A = \frac{24}{27}\frac{k\Delta d^3}{R} \tag{1.4}$$

Bibliography

[1] Obesity and overweight. *World Health Organization*, Fact sheet no. 311, 2015.

[2] Statistics Canada. Overweight and obese adults (self-reported), 2014. *Canadian Community Health Survey (CCHS)*, 2014.

[3] Haomiao Jia and Erica I Lubetkin. Trends in quality-adjusted life-years lost contributed by smoking and obesity. *American Journal of Preventive Medicine*, 38(2):138–144, 2010.

[4] Junghyo Jo, Oksana Gavrilova, Stephanie Pack, William Jou, Shawn Mullen, Anne E Sumner, Samuel W Cushman, and Vipul Periwal. Hypertrophy and/or hyperplasia: dynamics of adipose tissue growth. *PLoS Comput Biol*, 5(3):e1000324, 2009.

[5] Barbara Cannon and Jan Nedergaard. Developmental biology: neither fat nor flesh. *Nature*, 454(7207):947–948, 2008.

[6] Barbara Cannon and Jan Nedergaard. Brown adipose tissue: function and physiological significance. *Physiological Reviews*, 84(1):277–359, 2004.

[7] F Edmund Hunter. The Mitochondrion. Molecular Basis of Structure and Function. *Journal of the American Chemical Society*, 86(24):5704–5705, 1964.

[8] Paul Trayhurn and John H Beattie. Physiological role of adipose tissue: white adipose tissue as an endocrine and secretory organ. *Proceedings of the Nutrition Society*, 60(03):329–339, 2001.

[9] Vicente Gilsanz, Houchun H Hu, and Shingo Kajimura. Relevance of brown adipose tissue in infancy and adolescence. *Pediatric Research*, 73(1):3–9, 2012.

[10] Bruno Halpern, Marcio Correa Mancini, and Alfredo Halpern. Brown adipose tissue: what have we learned since its recent identification in human adults. *Arquivos Brasileiros De Endocrinologia & Metabologia*, 58(9):889–899, 2014.

[11] D. C. Berry, D. Stenesen, D. Zeve, and J. M. Graff. The developmental origins of adipose tissue. *Development*, 140(19):3939–49, 2013.

[12] Sung Sik Choe, Jin Young Huh, In Jae Hwang, Jong In Kim, and Jae Bum Kim. Adipose tissue remodeling: its role in energy metabolism and metabolic disorders. *Frontiers in Endocrinology*, 7, 2016.

[13] Marisa Coelho, Teresa Oliveira, and Ruben Fernandes. Biochemistry of adipose tissue: an endocrine organ. *Archives of Medical Science*, 9(2):191–200, 2013.

[14] Jeffrey L Halaas, Ketan S Gajiwala, Margherita Maffei, Steven L Cohen, et al. Weight-reducing effects of the plasma protein encoded by the obese gene. *Science*, 269(5223):543, 1995.

[15] Stefan Lehr, Sonja Hartwig, and Henrike Sell. Adipokines: a treasure trove for the discovery of biomarkers for metabolic disorders. *PROTEOMICS-Clinical Applications*, 6(1):91, 2012.

[16] B Perry and Y Wang. Appetite regulation and weight control: the role of gut hormones. *Nutrition & Diabetes*, 2(1):e26, 2012.

[17] Jennifer H Stern, Joseph M Rutkowski, and Philipp E Scherer. Adiponectin, Leptin, and Fatty Acids in the Maintenance of Metabolic Homeostasis through Adipose Tissue Crosstalk. *Cell Metabolism*, 23(5):770–784, 2016.

[18] Aimin Xu, Yu Wang, Hussila Keshaw, Lance Yi Xu, Karen SL Lam, and Garth JS Cooper. The fat-derived hormone adiponectin alleviates alcoholic and nonalcoholic fatty liver diseases in mice. *The Journal of Clinical Investigation*, 112(1):91–100, 2003.

[19] Wenwen Zeng, Roksana M Pirzgalska, Mafalda MA Pereira, Nadiya Kubasova, Andreia Barateiro, Elsa Seixas, Yi-Hsueh Lu, Albina Kozlova, Henning Voss, Gabriel G Martins, et al. Sympathetic neuro-adipose connections mediate leptin-driven lipolysis. *Cell*, 163(1):84–94, 2015.

[20] Eva Tomas, Tsu-Shuen Tsao, Asish K Saha, Heather E Murrey, Cheng cheng Zhang, Samar I Itani, Harvey F Lodish, and Neil B Ruderman. Enhanced muscle fat oxidation and glucose transport by ACRP30 globular domain: Acetyl–CoA carboxylase inhibition and AMP-activated protein kinase activation. *Proceedings of the National Academy of Sciences*, 99(25):16309–16313, 2002.

[21] V. Dubois, T. Jarde, L. Delort, H. Billard, D. Bernard-Gallon, E. Berger, A. Geloen, M. P. Vasson, and F. Caldefie-Chezet. Leptin induces a prolifera-

tive response in breast cancer cells but not in normal breast cells. *Nutrition and Cancer*, 66(4):645–55, 2014.

[22] G. Li, L. Cong, J. Gasser, J. Zhao, K. Chen, and F. Li. Mechanisms underlying the anti-proliferative actions of adiponectin in human breast cancer cells, MCF7-dependency on the cAMP/protein kinase-A pathway. *Nutrition and Cancer*, 63(1):80–8, 2011.

[23] Abebe Akalu and Peter C Brooks. Matrix, extracellular and interstitial. *Reviews in Cell Biology and Molecular Medicine*, 2005.

[24] Francesca Gattazzo, Anna Urciuolo, and Paolo Bonaldo. Extracellular matrix: a dynamic microenvironment for stem cell niche. *Biochimica et Biophysica Acta (BBA)-General Subjects*, 1840(8):2506–2519, 2014.

[25] Pekka Laurila and Ilmo Leivo. Basement membrane and interstitial matrix components form separate matrices in heterokaryons of PYS-2 cells and fibroblasts. *Journal of Cell Science*, 104(1):59–68, 1993.

[26] Hynda K Kleinman, Mary L McGarvey, John R Hassell, Vicki L Star, Frances B Cannon, Gordon W Laurie, and George R Martin. Basement membrane complexes with biological activity. *Biochemistry*, 25(2):312–318, 1986.

[27] Jamshid Khoshnoodi, Vadim Pedchenko, and Billy G Hudson. Mammalian collagen IV. *Microscopy Research and Technique*, 71(5):357–370, 2008.

[28] Tae-Hwa Chun. Peri-adipocyte ECM remodeling in obesity and adipose tissue fibrosis. *Adipocyte*, 1(2):89–95, 2012.

[29] Hynda K Kleinman, Mary L McGarvey, Lance A Liotta, Pamela Gehron Robey, Karl Tryggvason, and George R Martin. Isolation and characterization of type IV

procollagen, laminin, and heparan sulfate proteoglycan from the EHS sarcoma. *Biochemistry*, 21(24):6188–6193, 1982.

[30] Chris S Hughes, Lynne M Postovit, and Gilles A Lajoie. Matrigel: a complex protein mixture required for optimal growth of cell culture. *Proteomics*, 10(9):1886–1890, 2010.

[31] Hynda K Kleinman and George R Martin. Matrigel: basement membrane matrix with biological activity. In *Seminars in cancer biology*, volume 15, pages 378–386. Elsevier, 2005.

[32] Gabriel Benton, Hynda K Kleinman, Jay George, and Irina Arnaoutova. Multiple uses of basement membrane-like matrix (BME/Matrigel) in vitro and in vivo with cancer cells. *International Journal of Cancer*, 128(8):1751–1757, 2011.

[33] GS Themistocleous, H Katopodis, A Sourla, P Lembessis, CJ Doillon, PN Soucacos, and M Koutsilieris. Three-dimensional type I collagen cell culture systems for the study of bone pathophysiology. *In Vivo*, 18(6):687–696, 2004.

[34] Thomas Gutsmann, Georg E Fantner, Manuela Venturoni, Axel Ekani-Nkodo, James B Thompson, Johannes H Kindt, Daniel E Morse, Deborah Kuchnir Fygenson, and Paul K Hansma. Evidence that collagen fibrils in tendons are inhomogeneously structured in a tubelike manner. *Biophysical Journal*, 84(4):2593–2598, 2003.

[35] Matthew D Shoulders and Ronald T Raines. Collagen structure and stability. *Annual Review of Biochemistry*, 78:929, 2009.

[36] AG Nerlich, ML Nerlich, and PK Müller. Pattern of collagen types and molecular structure of collagen in acute post-traumatic pulmonary fibrosis. *Thorax*, 42(11):863–869, 1987.

[37] Sylvie Ricard-Blum. The collagen family. *Cold Spring Harbor Perspectives in Biology*, 3(1):a004978, 2011.

[38] Harvey Lodish, Arnold Berk, SL Zipursky, Paul Matsudaira, David Baltimore, James Darnell, et al. Collagen: the fibrous proteins of the matrix. *Molecular Cell Biology*, 4, 2000.

[39] Svetlana L Kotova, Peter S Timashev, Anna E Guller, Anatoly B Shekhter, Pavel I Misurkin, Victor N Bagratashvili, and Anna B Solovieva. Collagen structure deterioration in the skin of patients with pelvic organ prolapse determined by atomic force microscopy. *Microscopy and Microanalysis*, 21(02):324–333, 2015.

[40] Jan K Rainey, Chuck K Wen, and M Cynthia Goh. Hierarchical assembly and the onset of banding in fibrous long spacing collagen revealed by atomic force microscopy. *Matrix Biology*, 21(8):647–660, 2002.

[41] Vira V Artym and Kazue Matsumoto. Imaging Cells in Three-Dimensional Collagen Matrix. *Current Protocols in Cell Biology*, pages 10–18, 2010.

[42] MF Paige and MC Goh. Ultrastructure and assembly of segmental long spacing collagen studied by atomic force microscopy. *Micron*, 32(3):355–361, 2001.

[43] Klaus Kühn. Segment-long-spacing crystallites, a powerful tool in collagen research. *Collagen and Related Research*, 2(1):61–81, 1982.

[44] Romaine R Bruns, DJ Hulmes, Stephen F Therrien, and Jerome Gross. Procollagen segment-long-spacing crystallites: their role in collagen fibrillogenesis. *Proceedings of the National Academy of Sciences*, 76(1):313–317, 1979.

[45] Max Born and Emil Wolf. *Principles of optics: electromagnetic theory of propagation, interference and diffraction of light*. Elsevier, 1980.

[46] Yves F Dufrêne. Atomic force microscopy and chemical force microscopy of microbial cells. *Nature Protocols*, 3(7):1132–1138, 2008.

[47] Franz J Giessibl. AFM's path to atomic resolution. *Materials Today*, 8(5):32–41, 2005.

[48] Nader Jalili and Karthik Laxminarayana. A review of atomic force microscopy imaging systems: application to molecular metrology and biological sciences. *Mechatronics*, 14(8):907–945, 2004.

[49] Uroš Maver, Tomaž Velnar, Miran Gaberšček, Odon Planinšek, and Matjaž Finšgar. Recent progressive use of atomic force microscopy in biomedical applications. *TrAC Trends in Analytical Chemistry*, 80:96–111, 2016.

[50] Jian Zhong and Juan Yan. Seeing is believing: atomic force microscopy imaging for nanomaterial research. *RSC Advances*, 6:1103–1121, 2016.

[51] S Tripathy and EJ Berger. Measuring viscoelasticity of soft samples using atomic force microscopy. *Journal of Biomechanical Engineering*, 131(9):094507, 2009.

[52] Hans-Jürgen Butt, Brunero Cappella, and Michael Kappl. Force measurements with the atomic force microscope: Technique, interpretation and applications. *Surface Science Reports*, 59(1):1–152, 2005.

[53] Filomena A Carvalho and Nuno C Santos. Atomic force microscopy-based force spectroscopy–biological and biomedical applications. *IUBMB Life*, 64(6):465–472, 2012.

[54] Ignasi Jorba, Juan J. Uriarte, Noelia Campillo, Ramon Farré, and Daniel Navajas. Probing Micromechanical Properties of the Extracellular Matrix of Soft Tis-

sues by Atomic Force Microscopy. *Journal of Cellular Physiology*, 232(1):19–26, 2017.

[55] Jeffrey L Hutter and John Bechhoefer. Calibration of atomic-force microscope tips. *Review of Scientific Instruments*, 64(11):3342, 1993.

[56] Chuan Xu. Nanostructure and Nanomechanics of Collagen Self-Assemblies. *PhD Thesis, Memorial University of Newfoundland*, 2014.

[57] Heinrich Hertz. On the contact of elastic solids. *Journal Für Die Reine Und Angewandte Mathematik*, 92(110):156–171, 1881.

[58] KL Johnson, K Kendall, and AD Roberts. Surface energy and the contact of elastic solids. In *Proceedings of the Royal Society of London A: Mathematical, Physical and Engineering Sciences*, volume 324, pages 301–313. The Royal Society, 1971.

[59] Bharat Bhushan and Chetan Dandavate. Thin-film friction and adhesion studies using atomic force microscopy. *Journal of Applied Physics*, 87(3):1201–1210, 2000.

[60] Soma Das, PA Sreeram, and AK Raychaudhuri. A method to quantitatively evaluate the Hamaker constant using the jump-into-contact effect in atomic force microscopy. *Nanotechnology*, 18(3):035501, 2007.

Co-authorship Statement

This thesis was written by Zhe Dong, MSc student in the Merschrod group. The implemented changes were conducted based on feedback from Dr. Merschrod (Department of Chemistry, Memorial University), Dr. Christian (Department of Biochemistry, Memorial University), and Dr. Christian's student Niki Pallegar.

In Chapter 2, the experiment was designed by Drs. Christian and Merschrod, and Zhe Dong. The cell line culture, collagen overlays, and the measurements of leptin, adiponectin and triglycerides were conducted by Niki Pallegar. Zhe Dong collected the collagen matrices and analyzed the morphological and mechanical properties of the matrices with Atomic Force Microscopy (AFM). Zhe Dong also plotted and analyzed all the data, with assistance from Drs. Christian and Merschrod.

In Chapter 3, the 3D co-culture system was designed and built by Drs. Christian and Merschrod and Zhe Dong. The removal of Matrigel matrices was conducted by Zhe Dong. The morphological, mechanical properties of Matrigel matrices were measured by Zhe Dong, with AFM. Zhe Dong also solely performed the data collection, and the following analysis, with feedback from Dr. Merschrod.

Chapter 2

The interactions between native type I collagen matrix and adipocytes during adipogenesis

2.1 Motivation and summary

This project is in collaboration with Dr. Sherri Christian, Department of Biochemistry, Memorial university. Dr. Christian and her student, Niki Pallegar, carried out the cell culture on matrices which I prepared and provided, as well as the extraction and measurement of adipocyte secretion. I collected the matrices and analyzed the morphology and mechanics of the matrices by atomic force microscopy (AFM), including the testing and refinement of procedures for data collection and analysis. The data were jointly interpreted. I wrote this chapter with information, data, and feedback from Dr. Christian and Ms. Pallegar.

As discussed in Section 1.2, I altered native type I collagen monomer into a matrix as the artificial ECM in our 3D co-culture system. Hence, as the starting point, it is es-

sential to investigate the interactions between the collagen matrix and the adipocytes. Specifically, I compared the effects of two different collagen preparations (HANKS-collagen and PBS-collagen matrices) and the use of two different tissue culture plastics (tissue-culture treated and CellBind treated plates) on triglyceride accumulation, as well as leptin and adiponectin secretion. The morphology and elasticity of collagen matrices in the presence and absence of adipocytes were also measured by AFM.

Overall, I found that collagen overlays added to the developing adipocytes early during culture impaired secretion of adipokines from mature adipocytes with a greater effect on leptin than adiponectin. In addition, collagen prepared using phosphate buffered saline (PBS) had a greater suppression of leptin than adiponectin while collagen prepared using HANKS buffer suppressed secretion of both adipokines. The use of CellBind plates further suppressed leptin secretion with less effect on adiponectin secretion. In contrast, triglyceride accumulation was minimally impacted in any of the combinations. In addition, adipocytes altered collagen elasticity in a manner dependent both on adipocyte stage and the collagen preparation. Therefore, it is feasible to selectively manipulate the physiology and functionality of adipocytes by timing the addition of specific collagen overlays in combination with specific tissue-culture plates. These findings may have implications for analysis of adipocyte development *in vitro* as well as potential therapeutic applications to specifically alter adipocyte functionality.

2.2 Experimental

2.2.1 Cells and reagents

Our collaborators purchased the 3T3-L1 cell line from ATCC and confirmed it to be free of mycoplasma contamination using the MycoAlert test from Lonza (Switzerland).

All media and supplements were obtained from Invitrogen (Carlsbad, CA, USA) unless otherwise indicated. Cells were maintained in high-glucose DMEM supplemented with 10% newborn calf serum and 1% antibiotic/antimycotic (DMEM/NCS). To induce differentiation, cells were treated as previously described [1] in high-glucose DMEM supplemented with 10% fetal calf serum (DMEM/FBS). Dexamethasone (Dex) and 3-isobutyl-1-methylxanthine (IBMX) were obtained from Millipore (Billerica, MA, USA) and insulin from Sigma-Aldrich (St. Louis, MI, USA). FirbroCol collagen (Cat. no. 5133-A) was obtained from Advanced BioMatrix Inc (Carlsbad, CA, USA). Cells were cultured in tissue-culture (TC) treated 24-well plates (Falcon cat. no. 353226) or CellBind treated 24-well plates (Corning cat. no. 3337) as indicated. Media was changed every 2-3 days or as indicated.

2.2.2 Collagen matrices

Collagen was diluted to 3.3 mg/mL in PBS (1.9 mM NaH_2PO_4, 8.4 mM Na_2HPO_4, 137 mM NaCl, pH 7.2) or in 1X HANKS buffer (cat. no. 1910154, MP Biomedicals). Collagen in PBS (PBS-collagen) was neutralized to pH 7-7.5 by addition of HCl before addition to cells. Collagen in HANKS was neutralized by addition of HEPES (hydroxyethyl piperazineethanesulfonic acid, pH 7.2) to 250 mM (HANKS-collagen). Collagen solutions or control solutions lacking collagen (300 μL) were gently layered on top of the adipocytes and allowed to polymerize at 37 °C for 40 min. DMEM/FBS (1 mL) containing the additives appropriate for the stage of differentiation was added as indicated below.

2.2.3 Adipocyte physiology and functional characterization

Concentrations of leptin and adiponectin in the culture supernatant were determined using DuoSet ELISA kits specific for mouse from R&D Systems (Minneapolis, MN,

USA) following the manufacturer's instructions. Samples were analyzed in duplicate. Samples with concentrations falling below the detection limit of 62.5 pg/mL for the leptin ELISA are indicated as not detected (ND). Triglyceride accumulation was determined after removal of media and washing cells twice in PBS then resuspending in 1 ml PBS. Lipids from the resuspended cells were extracted using the Bligh-Dyer method [2], followed by additional manipulation as introduced in Appendix B.

2.2.4 Atomic Force Microscopy analysis

All of the AFM imaging and elasticity measurements were performed in contact mode in air, using a MFP-3D AFM (Asylum Research, Santa Barbara, CA). Chromium and gold coated silicon cantilevers with tips (CSC37/CR-AU from Mikromasch, USA) were employed. The resonance frequency and spring constant of the tips were about 20 kHz and 0.3 N/m, respectively. The specific value was determined by the thermal noise method [3] as implemented in the AFM software (Roger Proksch, Asylum Research). The elasticity (defined by Young's Modulus) was calculated using IGOR (Wavemetrics), which was also used for all AFM data collection and analysis. To extract Young's Modulus from the obtained force-distance curves, the Johnson-Kendall-Roberts (JKR) model [4], to adjust for the adhesion force between tip and sample, was chosen. To optimally protect the samples and assure the accuracy of the mechanics measurements, minimum nanoindentation [5] was performed and the JKR model was revised as Equation 1.3.

2.2.5 Statistical analysis

Statistical analysis was performed in R [6]. Differences were considered significant at $P<0.05$ and indicated by the asterisk (*).

2.2.6 Experimental details

Two sets of experiments were designed as illustrated in Figure 2.1.

In Exp. A (Figure 2.1A), we overlaid collagen matrix on top of adipocytes at the beginning of each differentiation stage: day 2, 4, 6. Day 2 was the beginning of the stage when pre-adipocytes started transforming into adipocytes. Day 4, with the addition of insulin to the wells, initiated the differentiation stage. Day 6 was when adipocytes almost finished differentiation and turned into mature adipocytes. I then removed the matrix on day 8. This operation let matrices stay in the cell culture media for 6, 4, or 2 days, respectively. Even though Exp. A can identify the interactions between collagen matrices and adipocytes during different stages of adipogenesis, it potentially confounded the results with an aging effect, in that the matrices were in media for different lengths of time. To eliminate the contributions of matrix aging, I also designed Exp. B, where the timing of additions were the same as Exp. A, but I removed and analyzed collagen matrices two days after each addition. This guaranteed the matrices were in media for the same, short period.

2.3 Results

2.3.1 Collagen matrices have different effects on adipocyte function when added at different stages of adipogenesis

I first determined if AFM can be used to observe a change in collagen morphology in response to culturing cells with collagen. The collagen was prepared in two different ways (described in Section 2.2.6) and overlaid on the 3T3-L1 pre-adipocytes. I obtained deflection images that show that both PBS-collagen and HANKS-collagen displays massive fibrous structure, demonstrating that fibrogenesis was successful with

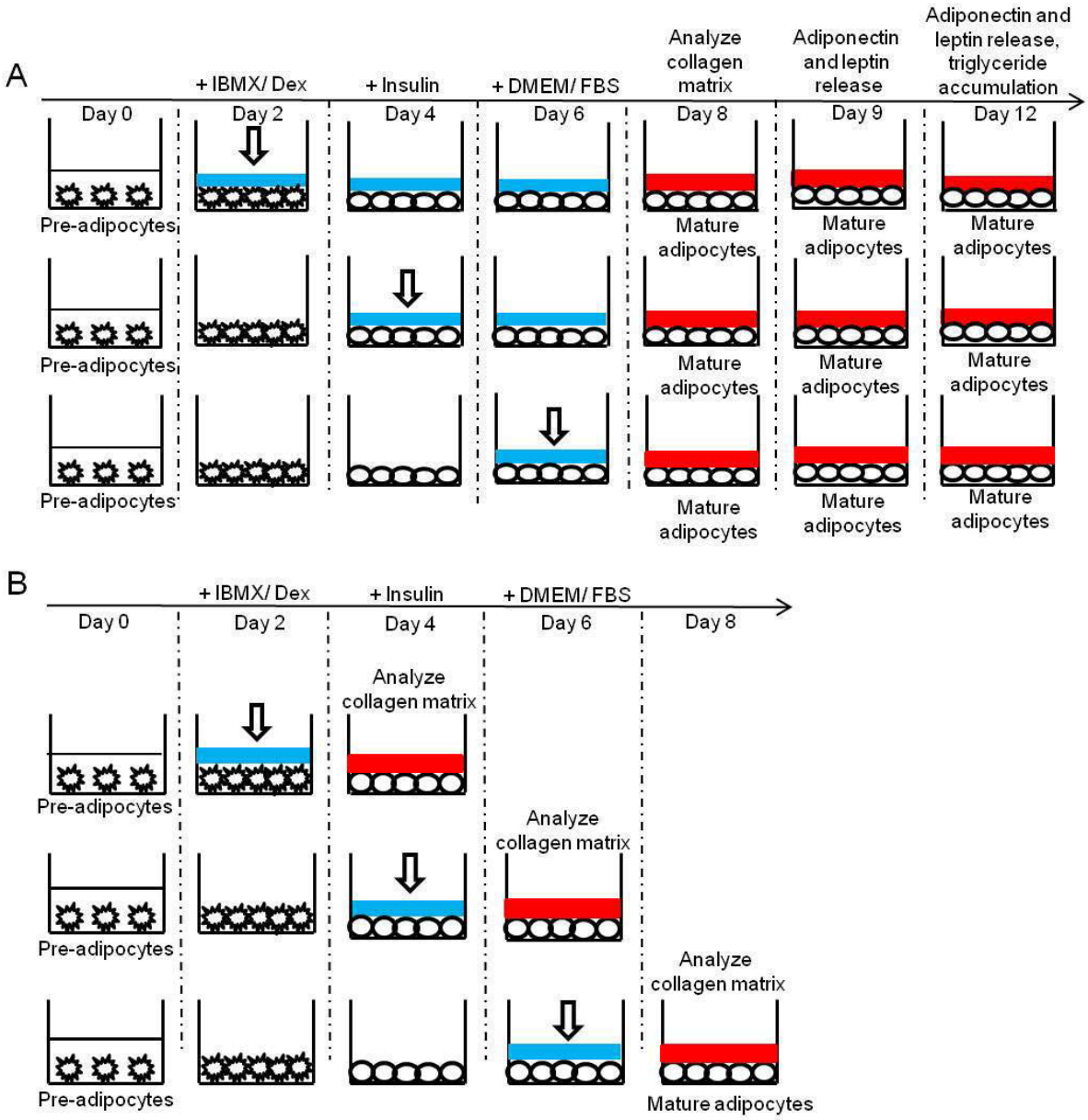

Figure 2.1: Schematic diagram of experiment A: the addition of collagen overlay to 3T3-L1 adipocytes at different stages of adipogenesis (Day 2, 4, 6) with analysis at day 8. Pre-adipocytes, prior to induction of differentiation, are indicated by the jagged circles while adipocytes that are undergoing adipogenesis are shown with smooth circles. The collagen layer is indicated by the thick line and added when indicated by the down-arrow. In parallel experiments, adiponectin and leptin concentrations were determined at day 9 or day 12 and triglyceride accumulation was determined at day 12. Experiment B: Collagen was added at different stages of adipogenesis and analyzed 2 days later.

both preparation methods (Figure 2.2). Moreover, the PBS-collagen matrix in contact with cells for 6 days tended to show thinner and less uniform fibers in comparison to the matrix when no cells were present (Figure 2.2 A-B). The HANKS-collagen displayed less distinct longer fibers than the PBS-collagen and was also modified in the presence of cells (Figure 2.2 C-D). Thus, I was able to observe the remodelling effect of the cells on the collagen matrices at the level of the fibers, with apparent effects on fibre geometry.

I then assessed the impact of the different collagen preparations on the physiology and function of the mature adipocytes. As an overall effect, collagen addition to cells led to a decrease in overall TG accumulation when all conditions were taken into account (Figure 2.3). For the effects of the specific collagen matrices, there was no significant effect of PBS-collagen on the total TG accumulation regardless of when the PBS-collagen was added. In contrast, the addition of HANKS-collagen on day 2, but not day 4 or 6, significantly reduced the overall accumulation of TG.

To analyze the effect of collagen matrix overlays on adipocyte function, we measured the amount of adiponectin and leptin secreted by the cells on day 9 and day 12 (Figure 2.4 and 2.5). The addition of either PBS-collagen or HANKS-collagen had an overall effect of suppressing adipokine secretion.

In the case of leptin, the suppression was greater when the collagen matrix was added earlier during adipogenesis with both PBS-collagen and HANKS-collagen, as leptin was not detectable when collagen matrix was added at the earliest timepoints (Figure 2.4). When collagen matrix was added at day 6, the suppression of leptin secretion was either absent or greatly reduced. Addition of collagen matrix at day 4 reduced leptin levels to not-detectable at day 9 and detectable but significantly suppressed with PBS-collagen at day 12. The lack of significant difference in leptin secretion when HANKS-collagen was added at day 4 and measured at day 9 is likely

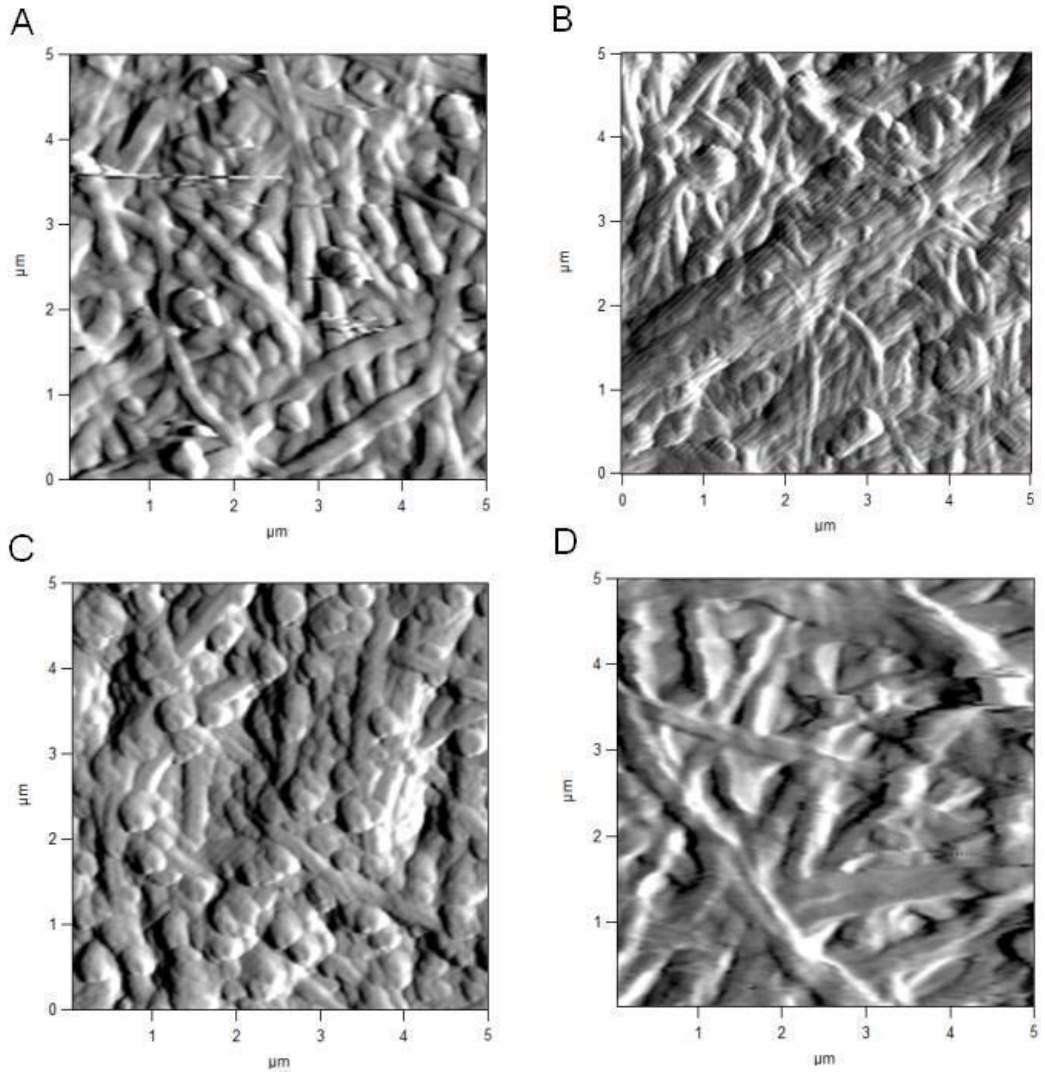

Figure 2.2: AFM images showing representative effects when collagen matrix is plated with adipocytes. The collagen matrix was layered on top of 3T3-L1 pre-adipocytes or into wells without cells for 6 days then analyzed by AFM. A) PBS-collagen in cell culture media without cells, or B) with adipocytes. C) HANKS-collagen in cell culture media or D) with adipocytes.

due to the variability seen in the control samples in combination with lower levels of leptin secretion. At day 9, the overall effect of PBS-collagen and HANKS-collagen matrices was statistically different whereas by day 12 both collagen matrices had similar effects.

In contrast, adiponectin secretion was affected more by the HANKS-collagen matrix at both days 9 and 12 when compared to the PBS-collagen matrix (Figure 2.5). Addition of HANKS-collagen at day 2 or day 4 resulted in a large and significant inhibition of adiponectin secretion at day 9 (Figure 2.5 A). At day 12 adiponectin levels remained significantly lower in adipocytes with HANKS-collagen at day 2 or 4 but clearly the adipocytes were able to regain some function as the difference in abundance is clearly reduced after the 3 additional days of maturation (Figure 2.5 B). Addition of PBS-collagen at day 4 significantly suppressed adiponectin secretion when added at day 12 but not at day 9 suggesting that PBS-collagen was able to reduce the maximum amount of adiponectin secreted with longer time cultures. Thus, HANKS-collagen ap-

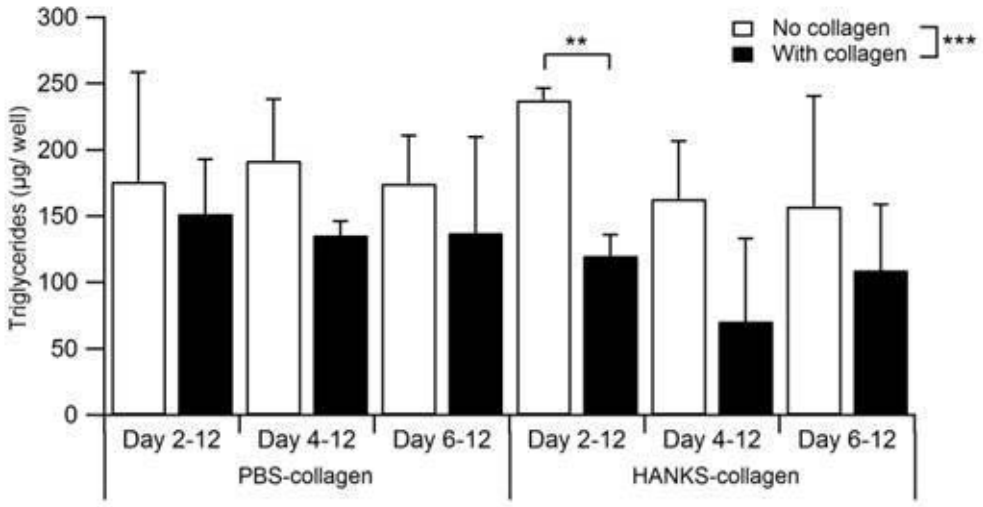

Figure 2.3: Total TG in 3T3-L1 cells at day 12 after adding collagen overlays at day 2, 4 or 6. Statistical analysis by 3-way ANOVA. *A priori* analysis of control vs. collagen at each stage by one tail Student's t-test [7]. *p$\leq$0.05, **p<0.01, ***p<0.001, shown are Mean $\pm$ Sem of 3 biological replicates.

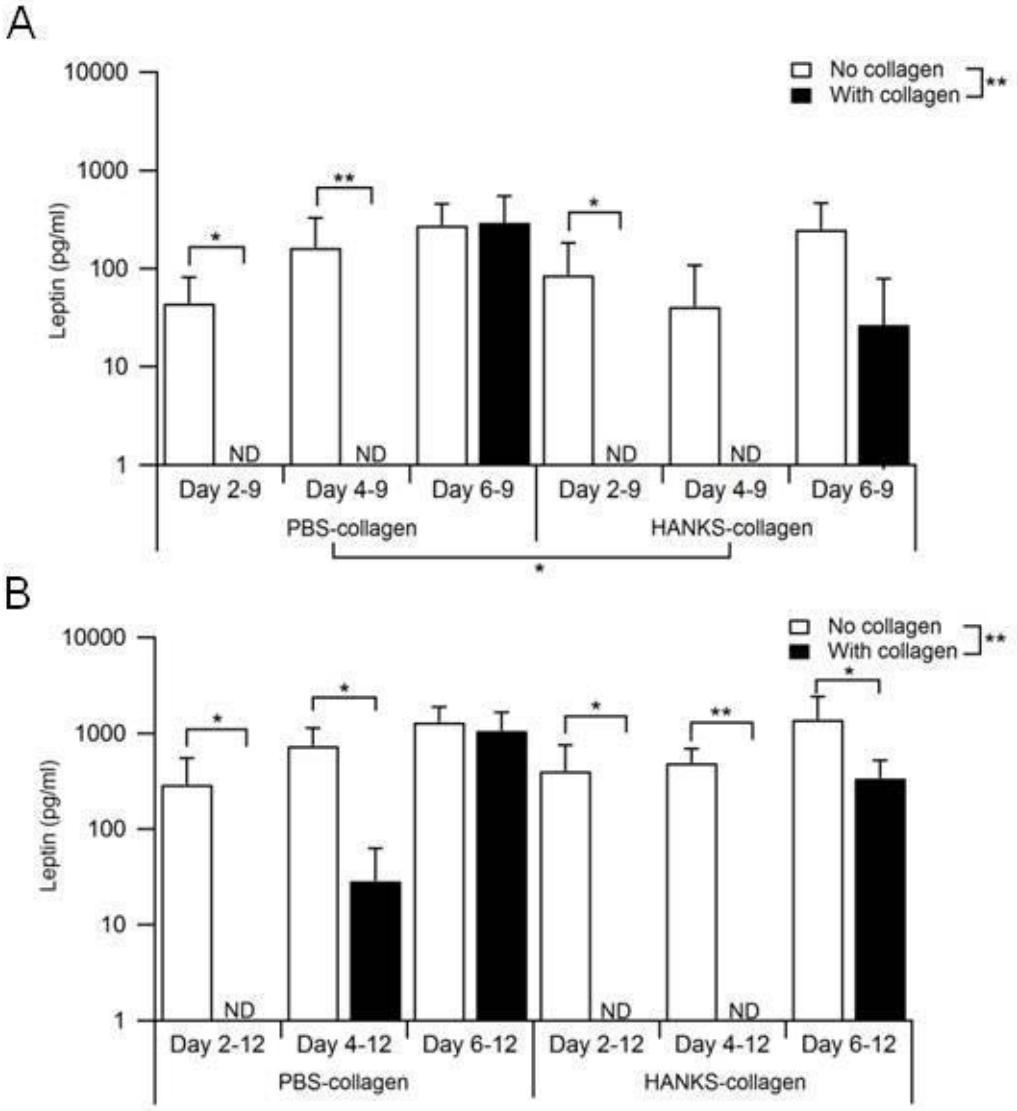

Figure 2.4: Leptin production is differentially affected by PBS-collagen and HANKS-collagen matrices when cells are plated on regular TC-treated plates. Levels of secreted leptin was determined at A) day 9 and B) day 12. Statistical analysis by 3-way ANOVA [8]. *A priori* analysis of control vs. collagen at each stage by Wilcoxon rank sum [9] for leptin levels as some samples were below the detection limit of the ELISA (ND: not detected; set to 2 pg/mL for ANOVA). *$p \leq 0.05$, **$p < 0.01$, ***$p < 0.001$, shown are Mean ± Sem of 3 biological replicates.

pears to more strongly support overall adipokine suppression while PBS-collagen has more selective suppressive effects.

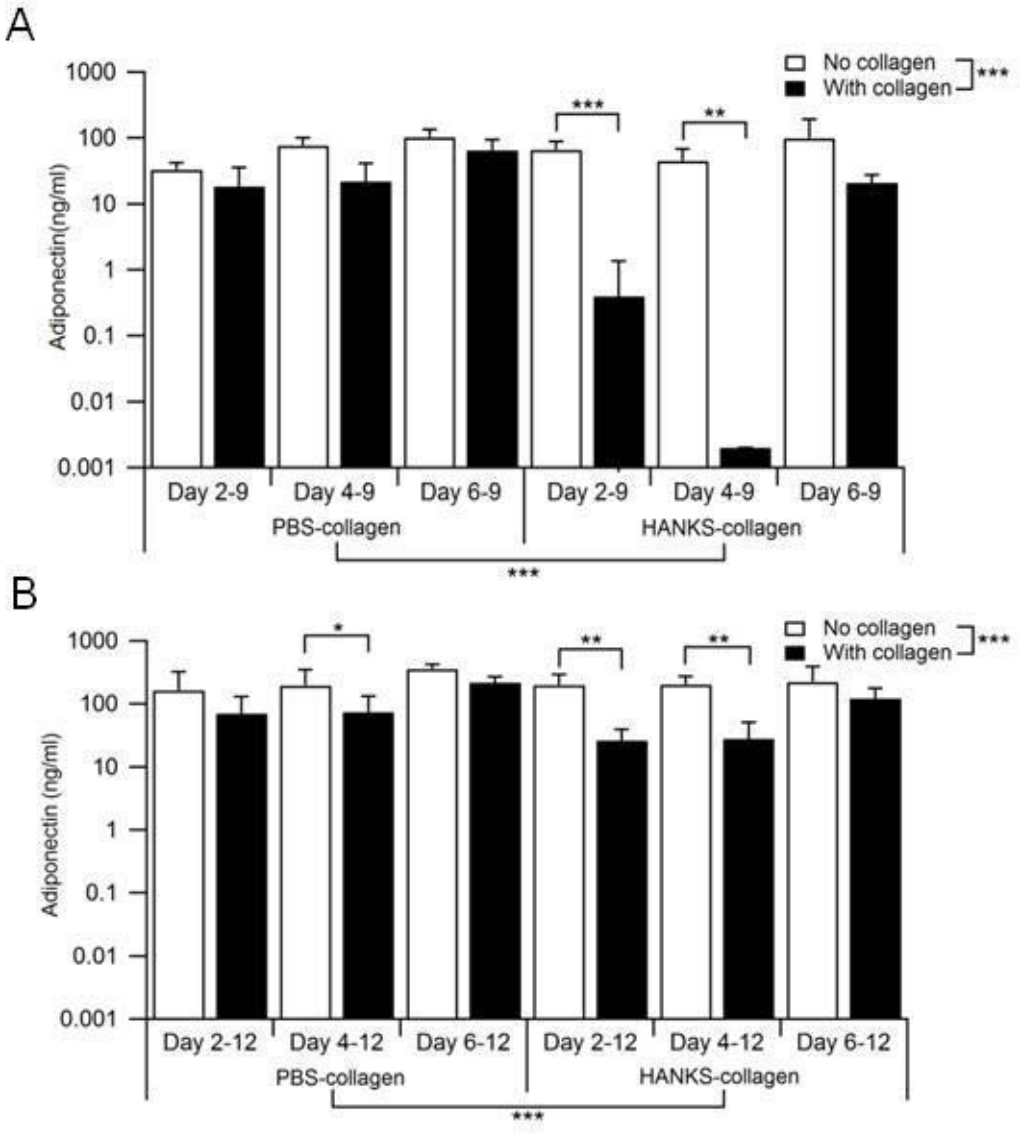

Figure 2.5: Adiponectin production is differentially affected by PBS-collagen and HANKS-collagen when cells are plated on regular TC-treated plates. A) Levels of secreted adiponectin was determined at day 9 B) day 12. Statistical analysis by 3-way ANOVA. *A priori* analysis of control vs. collagen at each stage by one tail Student's t-test. *$p \leq 0.05$, **$p < 0.01$, ***$p < 0.001$, shown are Mean ± Sem of 3 biological replicates.

2.3.2 Effect of CellBind plates on adipocyte physiology and function in the presence of collagen

All of the previous experiments were performed using typical tissue-culture treated plastic. However, culturing 3T3-L1 cells on specially treated dishes with higher levels of incorporated oxygen on the plastic, branded CellBind [10], can increase the ease of the adipogenesis assay as the cells remain more firmly attached. This effect is noticed particularly after I/D treatment when the cells round up at days 2-4 (S.L. Christian and N.K. Pallegar, unpublished observations). Therefore, we sought to determine if the addition of collagen overlays in combination with CellBind plates would further affect adipogenesis.

We first determined if CellBind plates affected adipocyte physiology or function in the absence of collagen. As expected, there was a significant increase in the amount of cellular TG and secreted leptin and adiponectin in cells induced to undergo adipogenesis compared to control (Neg) cells (Figure 2.6). There was an increase in TG accumulation when adipogenesis was induced in the CellBind plates (P=0.07). Although there appeared to be a modest decrease in adipokine secretion when cells were plated on CellBind plates, there was no significant effect of plate type for leptin secretion or adiponectin secretion. However, post-hoc analysis of adiponectin secretion revealed that on CellBind plates, there was an increase in spontaneous release of adiponectin, which caused there to be no significant difference in adiponectin secretion with adipogenesis measured at day 9 (Figure 2.6 C). However, overall CellBind plates do not significantly affect either TG accumulation or adipokine secretion.

We next determined the effect of the collagen matrices on TG accumulation and adipokine secretion when 3T3-L1 cells were cultured on CellBind plates (Figure 2.7). Similar to the regular TC-treated plates, my plots show an overall suppression effect of

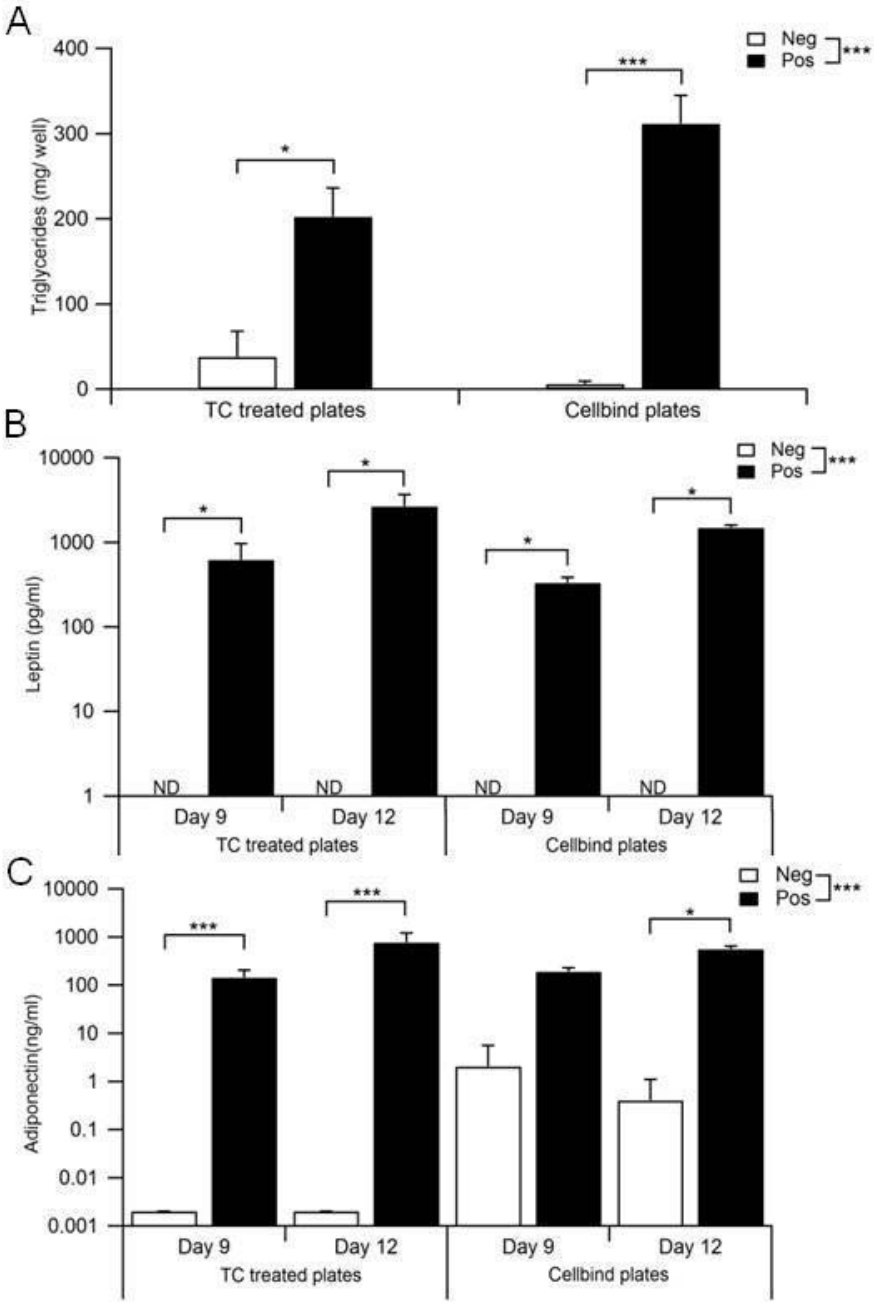

Figure 2.6: Adipogenesis is not significantly different when 3T3-L1 cells are cultured in regular tissue-culture (TC) treated dishes or CellBind dishes. A) TG accumulation at day 12, B) Leptin and C) adiponectin secretion at day 9 and 12 in cells culture on regular or CellBind plates in the absence (Neg) or presence (Pos) of adipogenic inducers. Statistical analysis by 2-way ANOVA [8]. *A priori* analysis of control vs. collagen at each stage by one tail Students' t-test for TG and Adiponectin and by Wilcoxon rank sum for leptin levels as some samples were below the detection limit of the ELISA (ND: not detected; set to 2 pg/ml for ANOVA). *$p \leq 0.05$, **$p < 0.01$, ***$p < 0.001$. Mean $\pm$ sem shown of 3 biological replicates.

collagen on TG accumulation when all conditions were taken into account. However, the only significantly different pairwise comparison was when PBS-collagen was added at day 4. Moreover, there was no overall significant difference between PBS-collagen and HANKS-collagen.

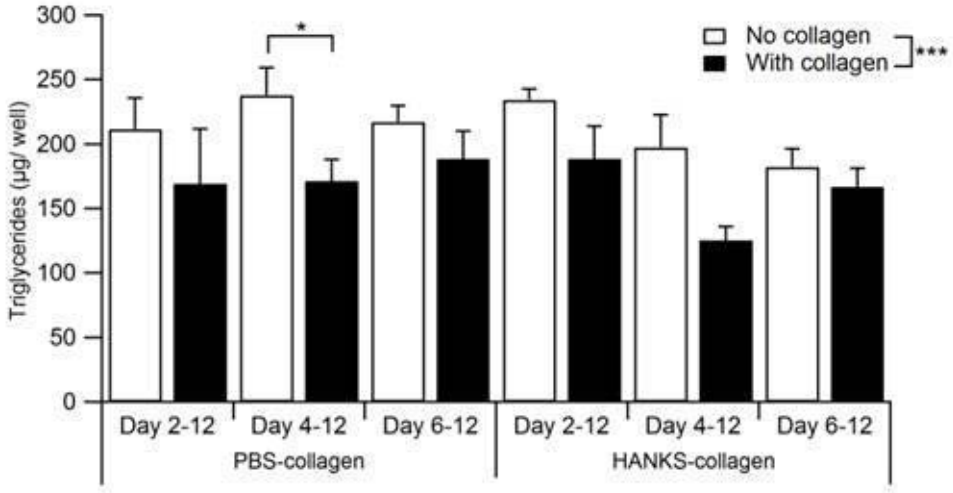

Figure 2.7: Total TG in 3T3-L1 cells at day 12 after adding collagen overlays at day 2, 4 or 6 on CellBind plates. Statistical analysis by 3-way ANOVA. *A priori* analysis of control vs. collagen at each stage by one tail Student's t-test. *$p \leq 0.05$, **$p < 0.01$, ***$p < 0.001$, shown are Mean ± Sem of 3 biological replicates.

In contrast, leptin levels after 9 days were particularly disrupted when cells were treated with either buffer or collagen during adipogenesis (Figure 2.8 A), suggesting that leptin secretion from cells grown on CellBind plates is more sensitive to disruption during adipogenesis. However, by day 12 the amount of leptin detected from the cells without collagen was similar to cells grown without disruption (Figure 2.6). Similar to the cells grown on TC-treated plates, adding PBS-Collagen or HANKS-Collagen at day 2 or day 4 resulted in a significant decrease in leptin but not when the collagen was overlaid at day 6 (Figure 2.8 B).

Even though there was an overall significant decrease in adiponectin levels by 2-way ANOVA (Figure 2.9), there was much less impact on the collagen overlays at either

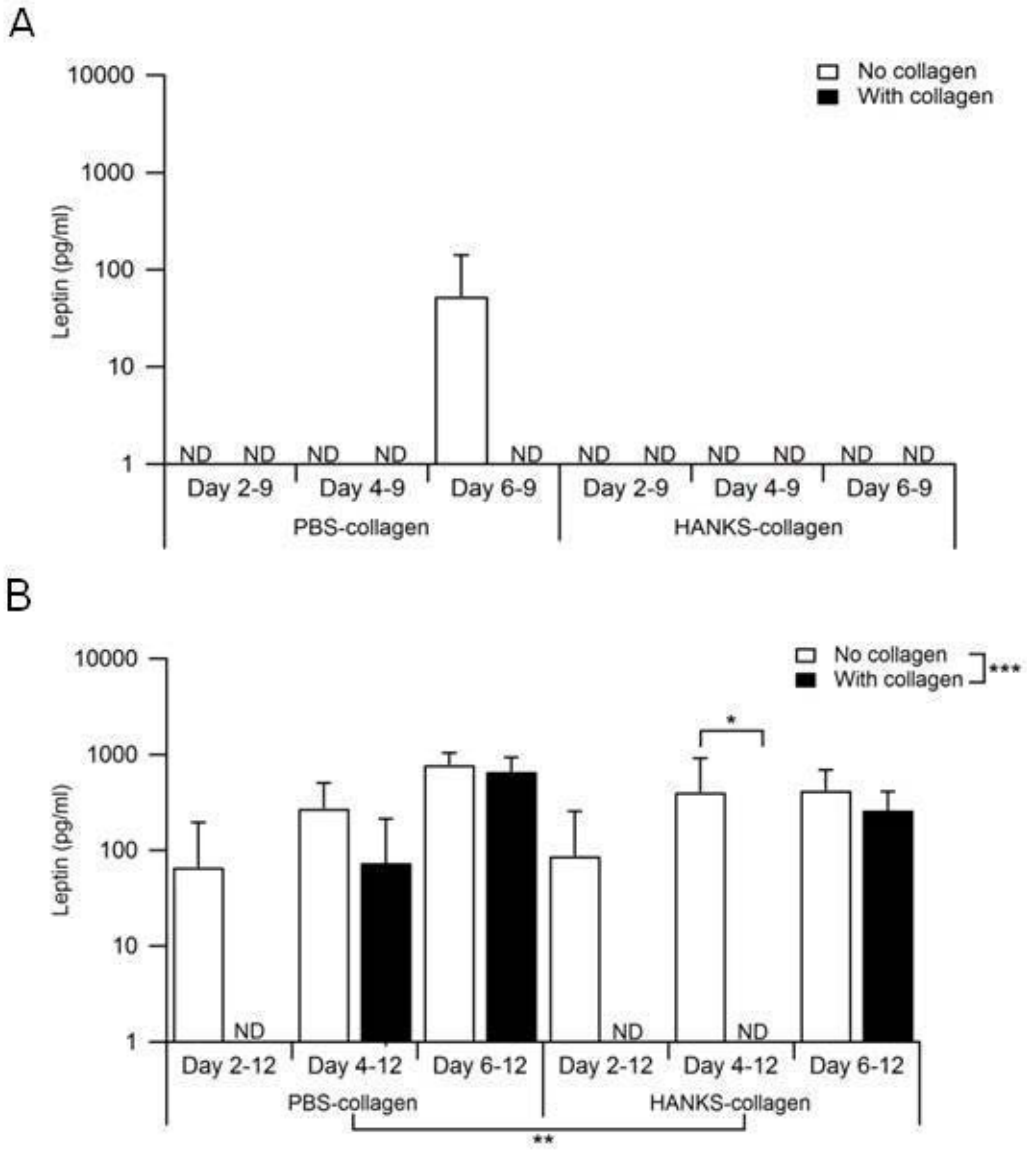

Figure 2.8: Leptin production is differentially affected by PBS-collagen and HANKS-collagen matrices when cells are plated on regular TC-treated plates. Levels of secreted leptin was determined at A) day 9 and B) day 12. Statistical analysis by 3-way ANOVA. *A priori* analysis of control vs. collagen at each stage by Wilcoxon rank sum for leptin levels as some samples were below the detection limit of the ELISA (ND: not detected; set to 2 pg/mL for ANOVA). *$p \leq 0.05$, **$p < 0.01$, ***$p < 0.001$, shown are Mean ± Sem of 3 biological replicates.

timepoint analyzed. Similar to the TC-treated plates, overlaying HANKS-collagen at day 4 resulted in a significant decrease in adiponectin secretion detected at both day 9 and day 12. Thus, overall culturing 3T3-L1 cells on CellBind plates in the presense of collagen matrices did not drastically change their physiology or function, however, leptin secretion was slightly more impacted with the CellBind plates, compared to TC-treated plates.

2.3.3 Stage-specific effects of developing adipocytes on collagen matrices

Since the addition of collagen at different stages of adipogenesis had different effects on TG, leptin, and adiponectin, I next determined if the collagen matrices were altered differently depending on the stage of the cells. To eliminate the possible effect of incubation time, I limited the incubation to 2 days in the presence or absence of cells at different stages of adipogenesis (Figure 2.1 B). I did not observe any major changes to the morphology of the collagen matrices when compared to without cells for 2 days at any stage (data not shown).

Therefore, I measured the Young's Modulus to assess the elasticity of the fibers to determine if more subtle molecular or supramolecular changes were taking place. Through the two-way ANOVA test, I found that when the PBS-collagen matrix was presented, either on TC treated or CellBind plates, the adipocytes did not overly impact the elasticity of collagen matrix (Figure 2.10 A,C). In contrast, with the HANKS-collagen I observed that, in general, the cells mechanically remodel the collagen matrix (Figure 2.10 B,D). More specifically, only when PBS-collagen was added on day 2, did the cells, which were cultured in CellBind plate, caused a decrease of collagen elasticity (Figure 2.10 C). With HANKS-collagen, the adipocytes caused changes to collagen elasticity when overlaid on day 6 regardless of which plate the cells were

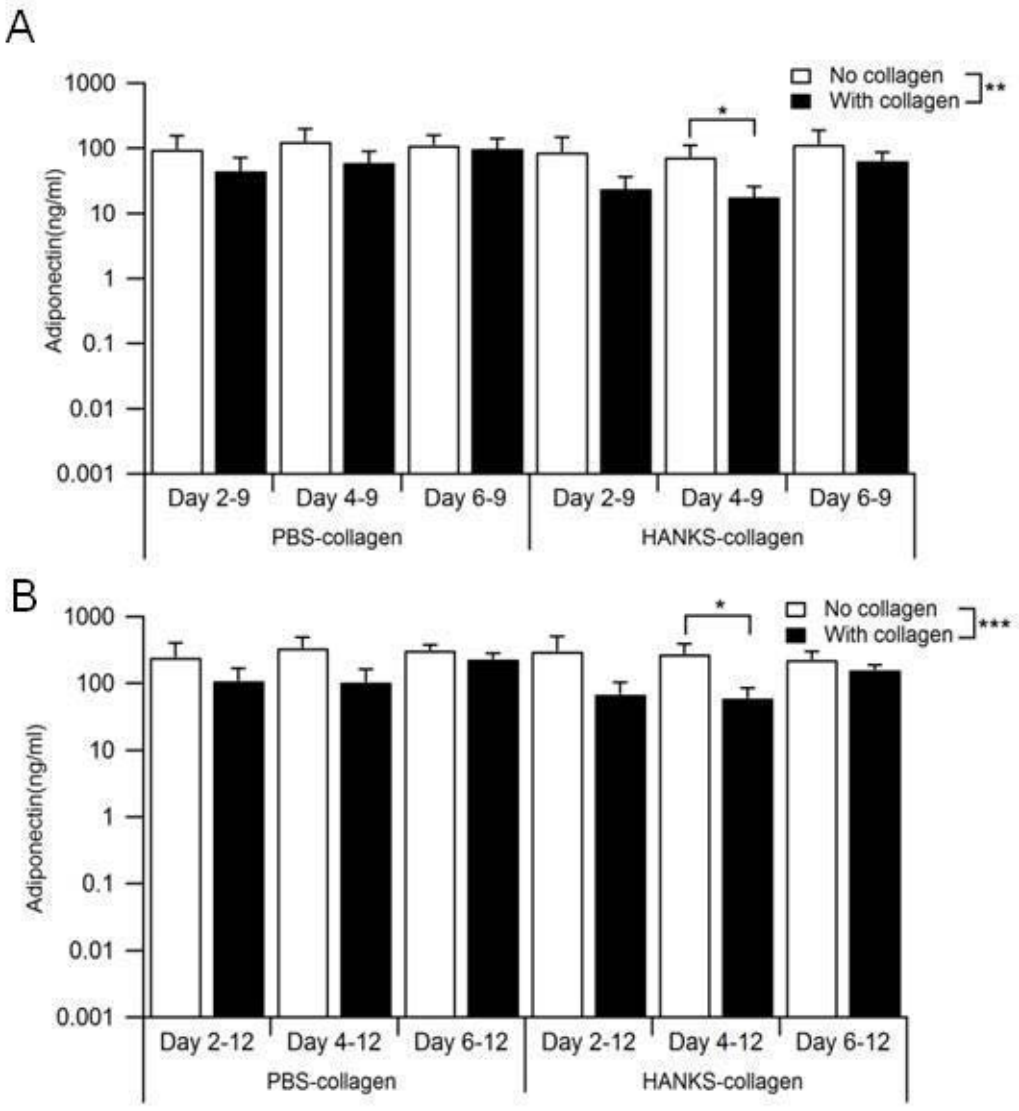

Figure 2.9: Adiponectin production is differentially affected by PBS-collagen and HANKS-collagen when cells are plated on regular TC-treated plates. Levels of secreted adiponectin was determined at A) day 9 and B) day 12. Statistical analysis by 3-way ANOVA. *A priori* analysis of control vs. collagen at each stage by t-test. *P$\leq$0.05, **P<0.01, ***P<0.001, shown are Mean $\pm$ Sem of 3 biological replicates.

grown on (Figure 2.10 B,D). In addition, with the CellBind plate, adding cells from day 2 to 4 also induced a change in collagen's elasticity (Figure 2.10 D). Interestingly, the results also showed that the elasticity of collagen matrices was affected when incubated during different stages of adipogenesis, even when cells were absent (Figure 2.10 B,D). Incubation of HANKS-collagen from day 4-6, in the presence of insulin in DMEM/FBS growth media, had a higher Young's Modulus than HANKS-collagen matrices incubated for the same amount of time but in the presence of IBMX/Dex (day 2-4) or just in FBS/DMEM growth media (day 6-8). Young's modulus measured on HANKS-collagen incubated on CellBind with FBS/DMEM growth media (day 6-8) was overall significantly different addition at the earlier stages. Therefore, minor adjustments in the media appear to affect the elasticity of collagen.

2.4 Discussion

The goal was to determine if overlay of collagen matrices would impact adipoctye physiology and function. We found that both the physiology and function of adipocytes could be differentially impacted by the addition of different collagen matrices in a manner that depended on when during adipogenesis the collagen overlays were applied. Moreover, the adipocytes modified the different collagen matrices differentially, which also depended on the adipocyte stage at which the collagen was overlaid.

Overall TG accumulation was generally suppressed by the addition of both PBS-collagen and HANKS-collagen (Figure 2.3 and 2.7). However, only two timepoints showed a specific reduction in TG accumulation when compared to buffer alone, with none of the changes particularly substantial. Thus, the collagen matrix overlays do not substantially alter the normal accumulation of lipid, the major physiological outcome of adipogenesis and its most visually obvious outcome. It is unknown if the modest

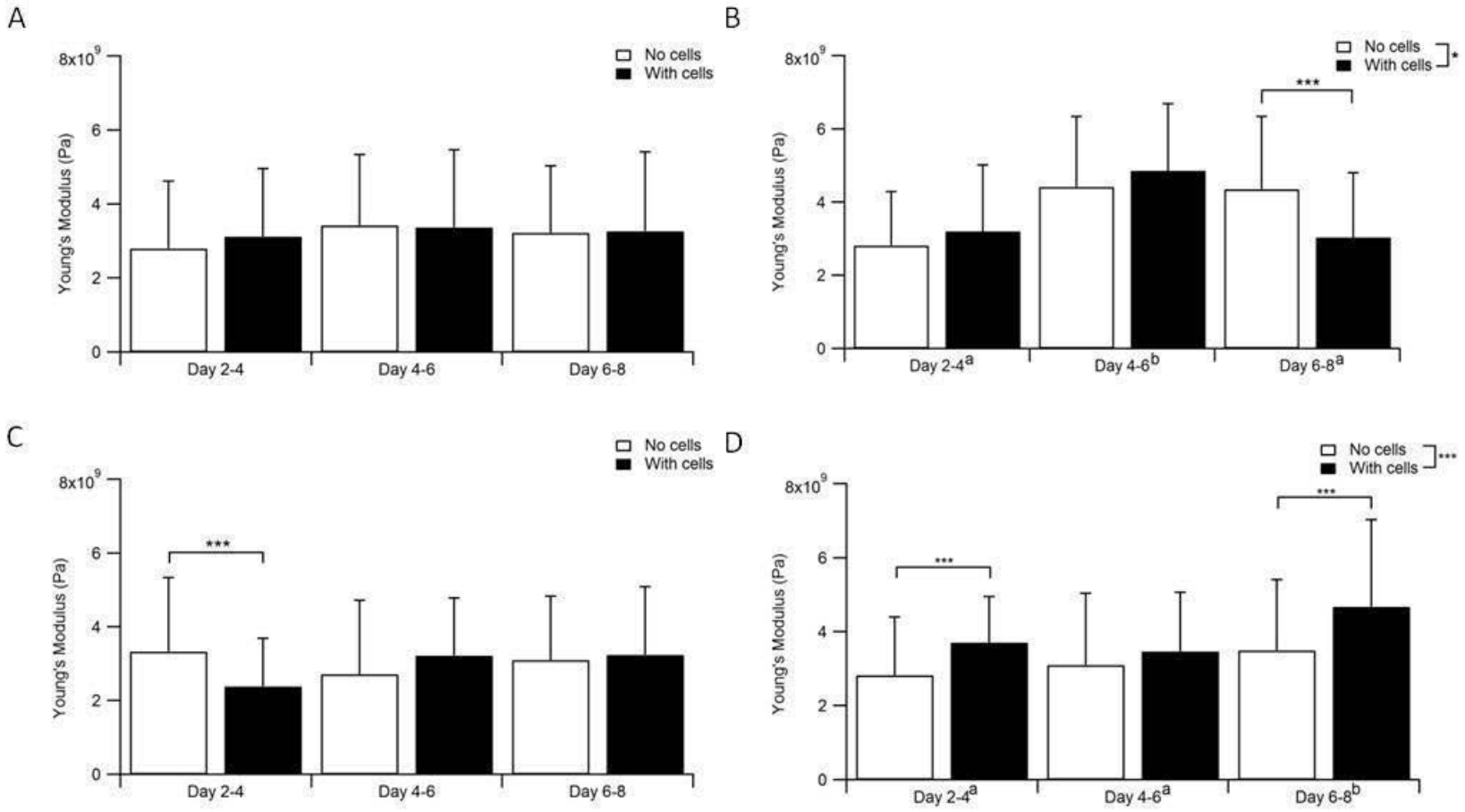

Figure 2.10: Elasticity (represented by Young's Modulus) of fibers on collagen matrix is differentially affected by adipocytes at different stages of differentiation. A) PBS-collagen plated in TC treated plates. B) HANKS-collagen plated in TC treated plates. C) PBS-collagen plated in CellBind plates. D) HANKS-collagen plated in CellBind plates. Different lower case letters indicate groups found to be statistically different by 2-way ANOVA.*$p \leq 0.05$, **$p < 0.01$, ***$p < 0.001$

decreases in TG accumulation would translate to biologically relevant outcomes if this experimental design could be modified to be tested *in vivo*.

However, investigation into adipocyte function, with respect to adipokine secretion revealed that both leptin and adiponectin can be affected by both the method of collagen matrix preparation and the type of cell culture plate used. I do not believe that the reduction in adipokine detection is due to physical interference of collagen to block the passage of secreted proteins. Leptin has a calculated mass of approximately 19 kDa protein while adiponectin has a calculated mass of 26 kDa. Since leptin was impacted more than adiponectin it is unlikely that the collagen matrices are reducing the passage of secreted proteins based on size.

Adiponectin is glycosylated at at least 6 sites [11, 12] whereas post-translational modifications of leptin, with the exception of disulfide bonds, have not been reported. The predicted pI of leptin is 5.85, while the predicted pI of unmodified adiponectin is 5.57 suggesting that different charges on the unmodified proteins of -2.5 and -6.4, respectively, could potentiate charge-charge interactions between the adipokine and collagen. In fact, an interaction with adiponectin and collagen has been reported previously *in vitro* and in injured but not healthy blood vessels *in vivo* [13]. However, leptin has not been reported to interact with collagen. Moreover, equivalent amounts of leptin and adiponectin were detected when the collagen was added to more mature cells (i.e. at day 6) and detected at both day 9 and 12 (Figure 2.3 and 2.7). Thus, there is no evidence to suggest that the collagen matrices physically impede the release of adipokines into the surrounding media.

Leptin was particularly and strongly affected by the addition of both types of collagen matrices. Strikingly, addition of collagen at the earliest stage of adipogenesis (day 2) resulted in leptin secretion that was, in many cases, below the level of detection. Thus, addition of collagen during active differentiation decreases leptin secretion

in a manner that is not readily reversible. Leptin expression is regulated by a variety of transcription factors including C/EBPα, SREBP1, and FosL1 during adipogenesis [14–16]. In addition, leptin expression is promoted by insulin, glucocorticoids, and even leptin itself [16]. The ability of collagen to impair leptin secretion when added at early stages of adipogenesis suggests that collagen may be specifically interfering with the action of one of these transcription factors. Whereas addition at later stages displayed significantly reduced interference with leptin synthesis, likely because the key transcription factors had already initiated leptin transcription.

In contrast to leptin, effects on adiponectin secretion were more modest and dependent on the collagen preparation. PBS-collagen had very little impact on adiponectin secretion while the HANKS-collagen, especially when associated with TC-treated plates decreased the secretion of adiponectin when added on the early stage of adipogenesis. Similar to leptin, the effect of collagen was greater when the collagen was added earlier during the differentiation process. Adiponectin expression is regulated by insulin via activation of PPAR-γ as well as by other transcription factors such as C/EBPα and negatively regulated by FoxO1 [17]. Thus, it appears that addition of HANKS-collagen, but not PBS-collagen, significantly impairs the regulation of transcription factors when added earlier during adipogenesis but that this effect is reduced when cells are cultured in CellBind plates. While it is clear that collagen overlays differentially regulate the appearance of adiponectin and leptin, the precise mechanism for this regulation will require further study.

Using AFM nanomechanics analysis I analyzed the effect of adipocytes on collagen focusing on stage-specific effects that occurred within 2-day windows during adipogenesis.

The fact that PBS-collagen was not remodeled by adipocytes could be ascribed to the elasticity of collagen. According to published results, the mechanics of ECM

plays a significant role in inducing adipocytes differentiation, especially the softer matrix can promote the adipogeneisis [18, 19]. Hence, due to the promotion of softer PBS-collagen, cells can smoothly finish adipogenesis; then less interactions took place between adipocytes and collagen fibers, which lead to the absence of remodeling. However, if the stiffer HANKS-collagen increased the local adhesion between cells and matrix, then cells would have to undergo more complex procedures to carry on the adipogenesis. The more work done by the cells during the adipogenesis, the more noticeable remodeling effects can be found. This also can explain why the secretion of adiponectin was not overly effected by the addition of PBS-collagen.

More specifically, on the first stage, the remodeling (labeled with *) can be found only when CellBind plate was involved (Figure 2.10 C,D). This is because at this stage, the pre-adipocytes were converting to adipocytes, so they tended to aggregate at the bottom of the well. Therefore, they would be more sensitive to the attaching strength of the plate. In contrast, the last stage, when adipocytes started to accumulate TG, which appears as fat droplets, they would tend to float in the cell culture media and stay closer to the matrix. Then more interaction could take place, which lead to the more drastic remodeling effect. This explains why when we compared the last stage, only on HANKS collagen the remodeling (labeled with *) can be found (Figure 2.10 B,D). Therefore, I can conclude that at the early stage, the property of plates dominates the adipogenesis; however, at the late stage, the adipogenesis will be impacted more by the matrix properties. Conversely, at the middle stage, no remodeling effect can be found. More research is required to explain this special middle stage. What should be taken into consideration is that the addition of insulin initiates the synthesis of TG, which associates with many complex reactions.

It is not clear why the HANKS-collagen had more substantive effects than PBS-collagen on adipokine secretion. While I observed that the HANKS-collagen solidi-

fied at a slower rate than PBS-collagen, both were solidified completely within 24h. HANKS contains KCl, $CaCl_2$, $MgSO_4$, and glucose, which are absent in the PBS-collagen preparation. The differences in buffer compositions did not cause obvious changes to the collagen morphology or significant changes to the Young's modulus. However, I speculate that the addition of the divalent cations Mg^{2+} and Ca^{2+}, potentially along with glucose, could have altered the protein interactions to promote modification by the adipocytes. Future study will be necessary to disentangle the key factors that cause the functional changes to the collagen preparation.

Regardless of the mechanism, we have clearly shown that apparently minor manipulations to the preparation of Type 1 collagen can result in significant and specific alterations to adipocyte physiology and function. This technique will permit researchers to selectively alter adipokine secretion without significant alterations to the ability of adipocytes to store triglycerides. As many other cell types can be grown on collagen matrices, a co-culture system to analyze the differential effects of adipokines on other cell types without specific alteration to TG is also feasible using the collagen overlay system. For example, since leptin and adiponectin have opposing effects on breast cancer cell proliferation specific alteration to adipokine concentrations using the described method would allow analysis in the absence of close contact to TG-filled adipocytes to reveal novel interactions between these cell types [20]. Moreover, adapting this method to *in vivo* procedures could potentially be used to selectively modify appetite-regulating hormones without diminishing the essential role of adipocytes to store free fatty acids, which are toxic in high abundance or when deposited ectopically [21].

2.5 Conclusions

In summary, I found that the secretion of leptin and adiponectin can be selectively manipulated while not substantially impairing TG synthesis in developing adipocytes by use of different collagen preparations and cell culture plates. These effects were consistent with the degree of modification of the developing adipocytes on the collagen matrices and dependent when during adipogenesis the collagen was applied. These finding may allow researchers a new way to affect adjacent cells or tissue by selectively manipulating adipocyte function.

Bibliography

[1] N.C. Smith, N.A. Fairbridge, N.K. Pallegar, and S. L. Christian. Dynamic upregulation of CD24 in pre-adipocytes promotes adipogenesis. *Adipocyte*, 4(2):89–100, 2015.

[2] E Graham Bligh and W Justin Dyer. A rapid method of total lipid extraction and purification. *Canadian Journal of Biochemistry and Physiology*, 37(8):911–917, 1959.

[3] Jeffrey L Hutter and John Bechhoefer. Calibration of atomic-force microscope tips. *Review of Scientific Instruments*, 64(11):3342, 1993.

[4] KL Johnson, K Kendall, and AD Roberts. Surface energy and the contact of elastic solids. In *Proceedings of the Royal Society of London A: Mathematical, Physical and Engineering Sciences*, volume 324, pages 301–313. The Royal Society, 1971.

[5] Chuan Xu. Nanostructure and Nanomechanics of Collagen Self-Assemblies. *PhD Thesis, Memorial University of Newfoundland*, 2014.

[6] Ross Ihaka and Robert Gentleman. R: a language for data analysis and graphics. *Journal of Computational and Graphical Statistics*, 5(3):299–314, 1996.

[7] Narendra P Singh, Michael T McCoy, Raymond R Tice, and Edward L Schneider. A simple technique for quantitation of low levels of DNA damage in individual cells. *Experimental Cell Research*, 175(1):184–191, 1988.

[8] Gerald H Lunney. Using analysis of variance with a dichotomous dependent variable: An empirical study. *Journal of Educational Measurement*, 7(4):263–269, 1970.

[9] Frank Wilcoxon and Roberta A Wilcox. *Some rapid approximate statistical procedures*. Lederle Laboratories, 1964.

[10] A. M. P. Pardo, M. Bryhan, H. Krasnow, N. Hardin, M. Riddle, O. LaChance, P. Gagnon, Upton T., and D. S. Hoover. Corning® CellBIND® Surface: An Improved Surface for Enhanced Cell Attachment. *Technical Report*, pages 1–8, 2010.

[11] Ayanthi A Richards, Tim Stephens, Hayley K Charlton, Alun Jones, Graeme A Macdonald, Johannes B Prins, and Jonathan P Whitehead. Adiponectin multimerization is dependent on conserved lysines in the collagenous domain: evidence for regulation of multimerization by alterations in posttranslational modifications. *Molecular Endocrinology*, 20(7):1673–1687, 2006.

[12] Ayanthi A Richards, Michelle L Colgrave, Jialiang Zhang, Julie Webster, Fiona Simpson, Elaine Preston, Donna Wilks, Kyle L Hoehn, Matthew Stephenson,

Graeme A Macdonald, et al. Sialic acid modification of adiponectin is not required for multimerization or secretion but determines half-life in circulation. *Molecular Endocrinology*, 24(1):229–239, 2010.

[13] Y Okamoto, Y Arita, M Nishida, M Muraguchi, N Ouchi, M Takahashi, T Igura, Y Inui, S Kihara, T Nakamura, et al. An adipocyte-derived plasma protein, adiponectin, adheres to injured vascular walls. *Hormone and Metabolic Research*, 32(02):47–50, 2000.

[14] Stephen G Miller, Piet De Vos, Michele Guerre-Millo, Kenneth Wong, Thomas Hermann, Bart Staels, Michael R Briggs, and Johan Auwerx. The adipocyte specific transcription factor C/EBPalpha modulates human ob gene expression. *Proceedings of the National Academy of Sciences*, 93(11):5507–5511, 1996.

[15] Mark M Mason, Yufang He, Hui Chen, Michael J Quon, and Marc Reitman. Regulation of Leptin Promoter Function by Sp1, C/EBP, and a Novel Factor 1. *Endocrinology*, 139(3):1013–1022, 1998.

[16] Christiane D Wrann and Evan D Rosen. New insights into adipocyte-specific leptin gene expression. *Adipocyte*, 1(3):168–172, 2012.

[17] Adeeb Shehzad, Waqas Iqbal, Omer Shehzad, and Young Sup Lee. Adiponectin: regulation of its production and its role in human diseases. *Hormones (Athens)*, 11(1):8–20, 2012.

[18] Murat Guvendiren and Jason A Burdick. Stiffening hydrogels to probe short-and long-term cellular responses to dynamic mechanics. *Nature Communications*, 3:792, 2012.

[19] D Adam Young, Yu Suk Choi, Adam J Engler, and Karen L Christman. Stimulation of adipogenesis of adult adipose-derived stem cells using substrates that mimic the stiffness of adipose tissue. *Biomaterials*, 34(34):8581–8588, 2013.

[20] Roman Camarda, Alicia Y Zhou, Rebecca A Kohnz, Sanjeev Balakrishnan, Celine Mahieu, Brittany Anderton, Henok Eyob, Shingo Kajimura, Aaron Tward, Gregor Krings, et al. Inhibition of fatty acid oxidation as a therapy for MYC-overexpressing triple-negative breast cancer. *Nature Medicine*, 2016.

[21] Harold Bays, Lawrence Mandarino, and Ralph A Defronzo. Role of the adipocyte, free fatty acids, and ectopic fat in pathogenesis of type 2 diabetes mellitus: peroxisomal proliferator-activated receptor agonists provide a rational therapeutic approach. *The Journal of Clinical Endocrinology & Metabolism*, 89(2):463–478, 2004.

Chapter 3

Investigation of 3D co-culture system by using AFM

With the thorough understanding of the development of adipocytes and the interactions between adipocytes and our artificial ECM, I then built the 3D co-culture system. Hence, this chapter includes the preliminary results that I obtained on our 3D co-culture system, which consists of adipocytes, the breast cancer cells, and Matrigel matrices. To investigate more possible materials in the system (other than the type I collagen matrix that was introduced in Chapter 2), I adopted Matrigel as the matrix to offer a more physiological environment to the breast cancer cells in the system.

In this chapter, I will firstly present the morphology of sole Matrigel matrix, Matrigel matrix with adipocytes embedded, Matrigel matrix with the breast cancer cells embedded, and Matrigel with both adipocytes and the breast cancer cells. Secondly we will compare the four sub-systems in the aspect of mechanical properties. The result shows that the designs of four sub-systems are all successful; especially in that I can observe the active interactions between adipocytes and the breast cancer cells in

the co-culture system, both morphologically and mechanically. After this study, now I have more understanding about the interplay between Matrigel, adipocytes and the breast cancer cells. This can be the valuable reference when I build a more physiological system, where I incorporate both the type I collagen and Matrigel in the artificial ECM.

3.1 Experiment

The samples in this project were kindly provided by Dr. Sherri Christian, Assistant Professor in the Department of Biochemistry, Memorial University of Newfoundland.

The 3T3-L1 pre-adipocyte cell line was adopted and cultured in the same media as described in section 2.1.1. The cells were embedded into the diluted Matrigel matrix five days after they differentiated into mature adipocytes. For the co-culture system, the breast cancer cell line MDA-MB-231 was purchased and seeded in the Matrigel matrix at the same time when the adipocytes were embedded. For each set of subsystem, three parallel experiments were designed to guarantee the accuracy of our data.

Then after the sample preparation, the AFM morphological and mechanical measurements were performed within 24 hours. The AFM measurements also followed the procedures mentioned in section 2.1.4

3.2 Study on sole Matrigel matrix as the baseline data

To my knowledge, due to the complex composition of Matrigel [1], there is no standard morphological image I can refer to. Hence I decided to firstly measure the morphol-

ogy and mechanics of Matrigel matrix with AFM as the baseline data, for further comparison when the cells were added in the system.

From the perspective of morphology, the Matrigel matrix is relatively featureless, as shown in a typical image in Figure 3.1, which agrees with the expectation due to the large amount of type IV collagen [1]. Unlike the massive fibrous structure on the type I collagen matrix as shown in Figure 2.2, type IV collagen is a type of non-fibrillar collagen [2]. Hence I will use Figure 3.1 as the baseline image to compare the influence of the addition of adipocytes or breast cancer cells on the morphology of the matrix.

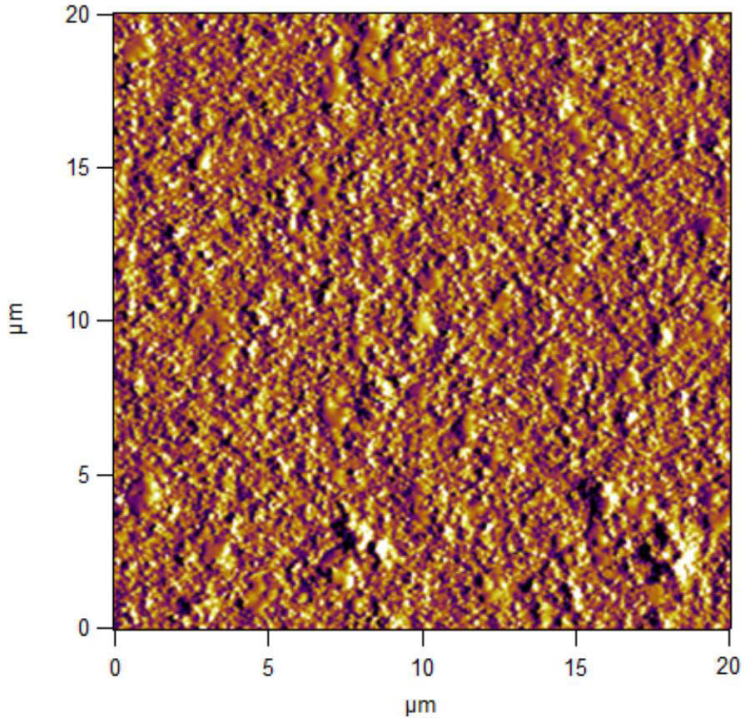

Figure 3.1: An AFM deflection image of a Matrigel matrix shows a relatively featureless surface

Secondly, regarding the mechanics of the Matrigel matrix, I quantified it by evaluating the Young's Modulus of the sample, through performing the AFM minimum nano-indentation. According to the box plot in Figure 3.2, the Young's Modulus of

the Matrigel matrix covers a wide range, between about 1.5 GPa to 5 GPa, which is also due to the complex composition of Matrigel. 50% of the data points fall in the box area, between 2 GPa and 4 GPa. The calculated average Young's Modulus is 3.049 GPa with the 1.440 GPa as the standard deviation. Hence, in the rest of the Chapter I will use these values as the reference to evaluate the effect from the adipocytes and/or the breast cancer cells to the Matrigel matrix.

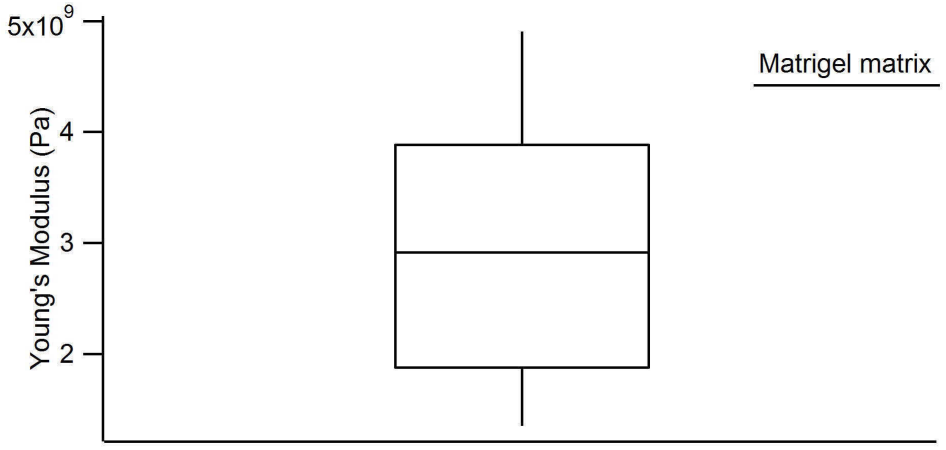

Figure 3.2: The box plot of the Young's Modulus of Matrigel matrix

3.3 Study on Matrigel matrix cultured with adipocytes

To avoid missing some distinct surface features and have a comprehensive understanding of the sample which has adipocytes embedded on Matrigel matrix, I started the imaging with a larger scanning size, 90 μm $\times$ 90 μm for each scan. When I scanned across it, instead of a featureless Matrigel surface, I came across many distinct features as shown in Figure 3.3 A. Many images were collected; here I illustrate the analysis using this image. On the top and middle of the figure, a number of protein clusters are present. Considering the featureless surface of Matrigel, the protein clusters may

result from the addition of adipocytes. Hence, they could be the cluster of the secretion of adipocytes, adipokines. Furthermore, on both the left and right sides of the figure, I spot some corrugated features with roughly 30 μm in diameter. Combined with the size of adipocytes reported in literature [3], those features are consistent with adipocytes. The striations are artifacts formed during the air-drying process during sample preparation.

A zoom of the marked rectangular area yields Figure 3.3 B, which clearly shows the geometry of the protein cluster which can be utilized for the future study to assign the particular adipokines. Also, the corrugated features spread all over the sample, indicates that the adipocytes were successfully cultured on the Matrigel matrix.

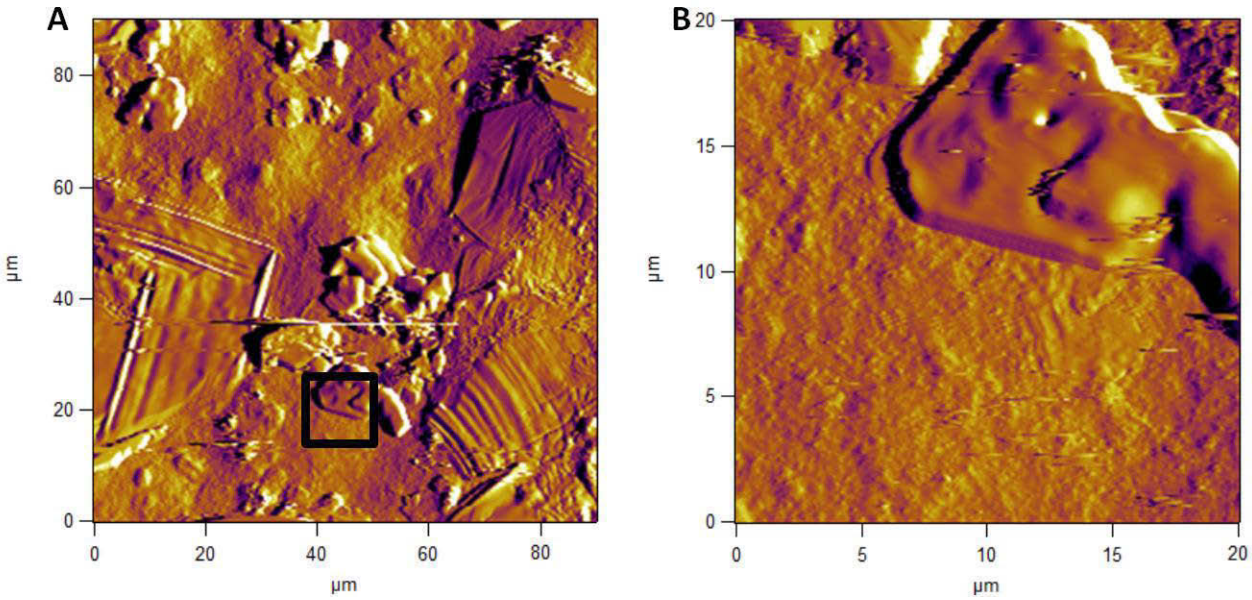

Figure 3.3: The AFM deflection image of Matrigel matrix with adipocytes. A: image at larger scale (90 μm on a side); B: zoom in at the selected area

With respect to mechanical properties, I measured the Young's Modulus of the sample and made a comparison with the sole Matrigel matrix. The result is shown in Figure 3.4. According to the plot, the sample of adipocytes on Matrigel matrix also shows widely distributed Young's Modulus. The p-value of the following one tail Stu-

dent t-test is less then 0.001, which confirms that the two sets of data are statistically different. This study shows that the addition of the adipocytes indeed caused the variation of the Matrigel's mechanics. Besides, the consistency of wide-spread Young's Modulus suggests the composition of Matrigel remains complex and heterogeneous after the the addition of adipocytes. Yet it does show an overall significant decreasing of the Young's Modulus of 2.310 ± 1.329 GPa. Hence, the addition of adipocytes can soften the Matrigel matrix in general. This finding corresponds well with one well known character of adipocytes, that they are cells with tremendously low elastic modulus, even in comparison with other mesenchymally-derived stem cells [4]. Then the addition of soft cells generally brings down the overall Young's Modulus of the sample.

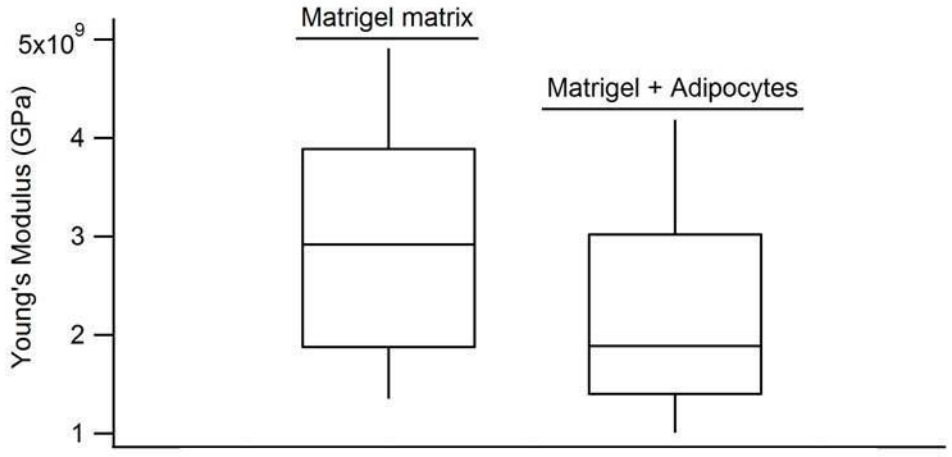

Figure 3.4: The comparison between the Young's Modulus of the Matrigel only, and the Matrigel with adipocytes.

3.4 Study on Matrigel matrix cultured with breast cancer cells

Similar to the last section, I firstly investigated the morphology of the breast cancer cell-embedded matrix by starting imaging with a larger length scale, 90 μm, as shown in Figure 3.5 A. The images present remarkably different structures in comparison to the Matrigel only and the Matrigel with adipocytes. On the matrix, some spindle-shaped convex structures exist and are surrounded by smaller clusters. Supported by the morphological assignments in the literature [5], I attribute the spindle-shaped structure to the MDA-MB-231 breast cancer cells. This AFM image also confirms the successful culture of the breast cancer cells on the Matrigel matrix. Then I continued to zoom in to a smaller area. As shown in image B, the breast cancer cell is surrounded by protein particles. Furthermore, the protein particles only distribute along the edges of the cell. Hence, the proteins could be the secretion of the breast cancer cells. Given the fact that during the invasion, the breast cancer cells secrete matrix metalloproteinases to consume the surrounding matrix [6], it is possible that the protein particles are matrix metalloproteinases and their products. However, future investigation is still required to prove this possibility.

After the existence of the breast cancer cells was confirmed by AFM images, we investigated how the breast cancer cells mechanically modified the Matrigel matrix. According to Figure 3.6, after the addition of breast cancer cells, the Young's Modulus of the sample spreads in a even wider range, and shifts toward higher values. Followed by a Student t-test, the two sets of data in Figure 3.6 are proved to be statistically different ($p=0.0068$). The increasing of Young's Modulus implies the cell behaviour of breast cancer cells stiffen the matrix. The findings in my project also agree with the established conclusions that the breast cancer cells can increase the heterogeneity

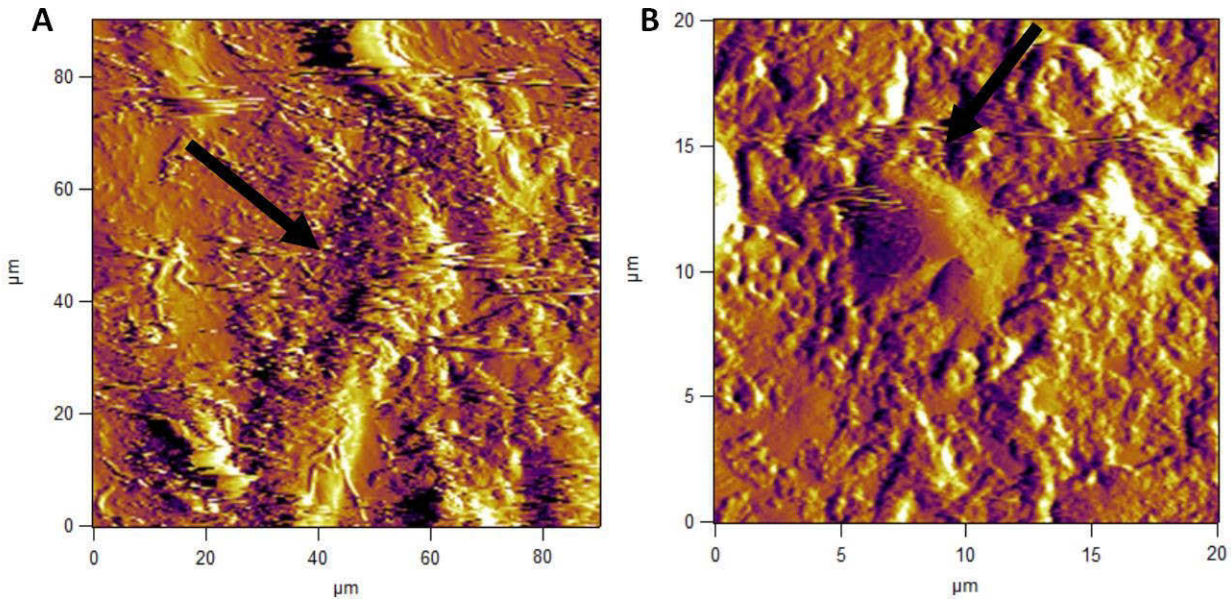

Figure 3.5: The AFM deflection image of Matrigel matrix with the breast cancer cells. A: image at larger scale (90 μm on a side); B: image at smaller scale (20 μm on a side).

of matrix Young's Modulus [7] and stiffen the surrounding tissues [8].

3.5 Study on Matrigel matrix cultured with the co-culture system

Eventually, I built the co-culture system, which has the adipocytes as the bottom layer, and the Matrigel with embedded cancer cells on top, as introduced in Figure 1.1. I was aiming to seek how the interactions between the adipocytes and breast cancer cells would change their appearance and mechanics.

An an example, the AFM deflection image in Figure 3.7 A shows the co-existence of two types of cultured cells. Noticeably, instead of being in spindle shapes as in Figure 3.5 A, the breast cancer cells adopt another spherical configuration and circularly distribute on the surface. According to Ivers et al. research [9], the co-culture of

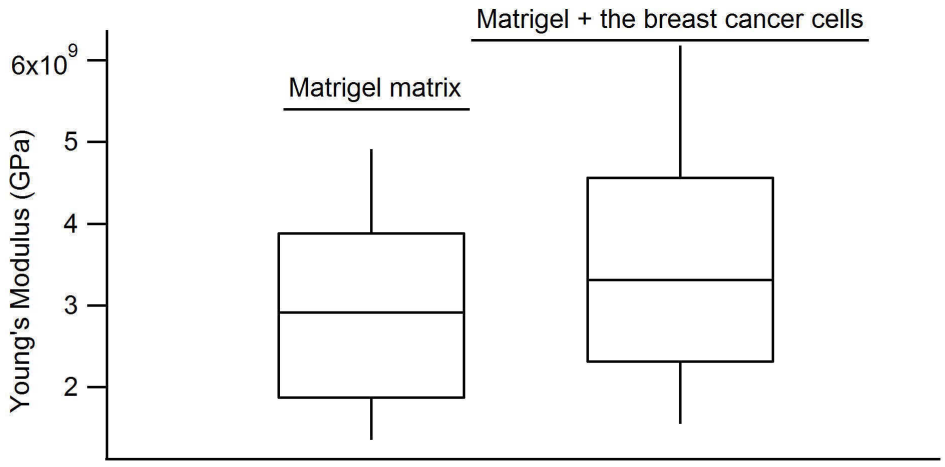

Figure 3.6: The comparison between the Young's Modulus of the Matrigel only, and the Matrigel with the breast cancer cells.

breast cancer cells and other epithelial cells tends to make breast cancer cells rounded up and aggregate around the epithelial cell, then eventually convert it into breast cancer cells. To have a clearer view, I zoomed in at the indicated area and obtained image B, where the corrugated structure indicated the existence of adipocytes, as discussed in the former section. The shape changing of breast cancer cells and the co-existence of two types of cells confirms that the co-culture system has been successfully established, and active interactions happened between adipocytes and breast cancer cells. Figure 3.8 shows a clearer rounded shape of the breast cancer cells.

Regarding the mechanical properties, it appears that as in Figure 3.9 the overall influence from the co-cultured cells to the matrix brought the Young's Modulus down, but still kept it in the similarly wide range. This is a balanced result after taking the addition of softer adipocytes and the stiffening effects of breast cancer cells into consideration. However, the general decrease of Young's Modulus indicates that the adipocytes and/or synergistic remodeling by the co-culture contributes more to the overall mechanics. The specific reason for this still needs further study.

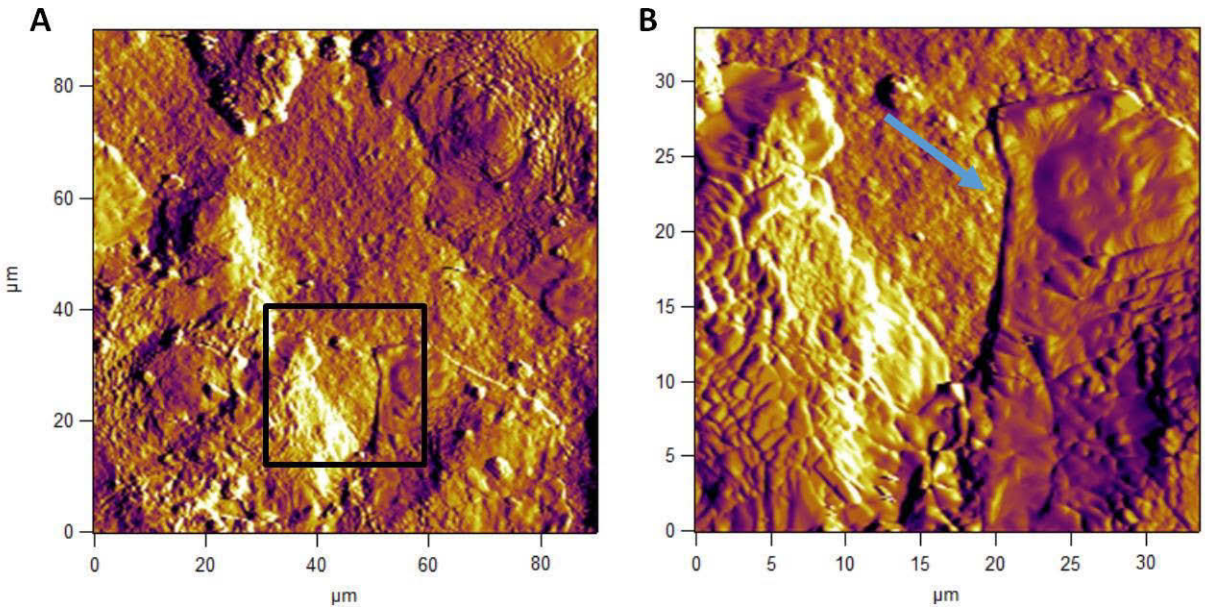

Figure 3.7: An AFM deflection image of the co-culture system. A: image at larger scale (90 μm); B: zoom-in at the selected area on image A

3.6 Conclusions

In this chapter, I carried out the first measurements of our 3D co-culture system, where the adipocytes and breast cancer cells actively interact and cause the change in both their morphologies and mechanics.

I obtained AFM images that showed adipocytes secreted some protein clusters, which are possibly the adipokines. The striated structures were suspected to be the remaining fat after drying out during sample preparation. On the contrary, the breast cancer cells were easier to be identified due to their spindle-like shape. We also observed the consequences of secreted matrix metalloproteinases around the breast cancer cells. In the co-culture sample, a noticeable shape changing, from spindle like to spherical shape, of breast cancer cells confirmed the active interactions between the two types of cells.

Mechanically, the addition of soft adipocytes decreased the Young's Modulus of

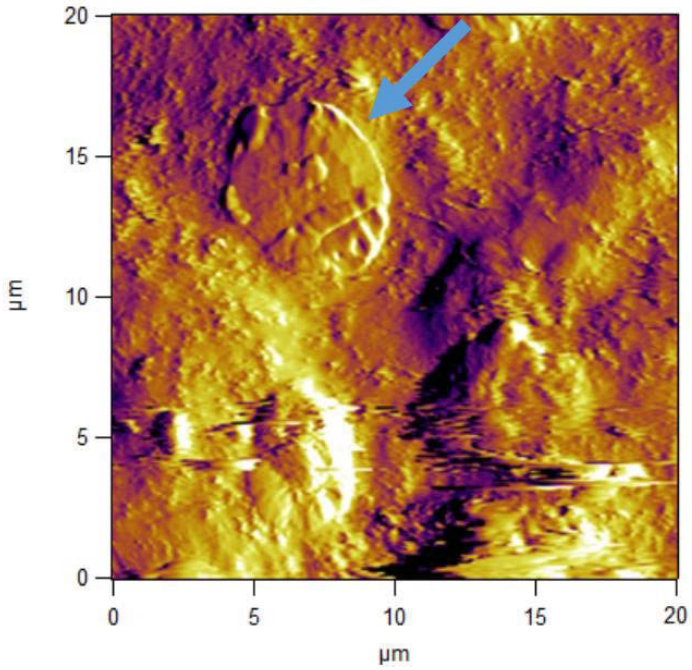

Figure 3.8: The AFM deflection image of the co-culture system that shows the rounded shape of the breast cancer cells

Matrigel matrix; however, the stiffening effect of breast cancer cells reversely increased it. The overall effect when we take both the cells into account showed a decrease in Young's Modulus.

Similar 3D co-culture systems with adipocytes and breast cancer cells have been built and investigated by other groups. For example, Balaban et al. [10] created a co-culture system and reported that the fatty acids released from adipocytes can be transferred to and utilized by the breast cancer cells to regulate their cell behaviours. And yet, to my knowledge this is the first time that both morphology and mechanics of the system is analysed by AFM. Nevertheless, there is still more investigation required to improve the system and thoroughly understand the interactions between these two types of cells. For example, instead of measuring the overall mechanics of the matrix, I can focus on the mechanics analysis of cells and cell secretions. A comparison of my results with reported values can help identify the protein clusters. After I build the

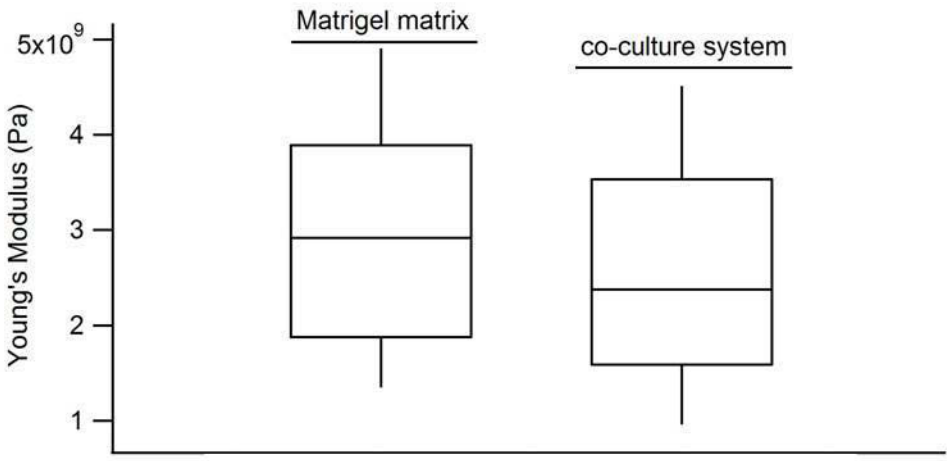

Figure 3.9: The comparison between the Young's Modulus of the Matrigel only, and the Matrigel with the co-culture system.

mechanics "database", I can perform a large force mapping on the co-culture sample, and directly observe the distribution of cells and furthermore, study their interactions.

Bibliography

[1] Chris S Hughes, Lynne M Postovit, and Gilles A Lajoie. Matrigel: a complex protein mixture required for optimal growth of cell culture. *Proteomics*, 10(9):1886–1890, 2010.

[2] Harikrishna Tanjore and Raghu Kalluri. The role of type IV collagen and basement membranes in cancer progression and metastasis. *The American Journal of Pathology*, 168(3):715–717, 2006.

[3] C Farnier, S Krief, M Blache, F Diot-Dupuy, G Mory, P Ferre, and R Bazin. Adipocyte functions are modulated by cell size change: potential involve-

ment of an integrin/ERK signalling pathway. *International Journal of Obesity*, 27(10):1178–1186, 2003.

[4] Eric M Darling, Matthew Topel, Stefan Zauscher, Thomas P Vail, and Farshid Guilak. Viscoelastic properties of human mesenchymally-derived stem cells and primary osteoblasts, chondrocytes, and adipocytes. *Journal of Biomechanics*, 41(2):454–464, 2008.

[5] Joseph M Gozgit, Brian T Pentecost, Sharon A Marconi, Christopher N Otis, Chuanyue Wu, and Kathleen F Arcaro. Use of an aggressive MCF-7 cell line variant, TMX2-28, to study cell invasion in breast cancer. *Molecular Cancer Research*, 4(12):905–913, 2006.

[6] Ling Wang, Yun Ling, Yan Chen, Cheng-Ling Li, Feng Feng, Qi-Dong You, Na Lu, and Qing-Long Guo. Flavonoid baicalein suppresses adhesion, migration and invasion of MDA-MB-231 human breast cancer cells. *Cancer Letters*, 297(1):42–48, 2010.

[7] Marija Plodinec, Marko Loparic, Christophe A Monnier, Ellen C Obermann, Rosanna Zanetti-Dallenbach, Philipp Oertle, Janne T Hyotyla, Ueli Aebi, Mohamed Bentires-Alj, Roderick YH Lim, et al. The nanomechanical signature of breast cancer. *Nature Nanotechnology*, 7(11):757–765, 2012.

[8] Arian Ansardamavandi, Mohammad Tafazzoli-Shadpour, Ramin Omidvar, and Iisa Jahanzad. Quantification of Effects of Cancer on Elastic properties of Breast Tissue by Atomic Force Microscopy. *Journal of the Mechanical Behavior of Biomedical Materials*, 2016.

[9] Laura P Ivers, Brendan Cummings, Funke Owolabi, Katarzyna Welzel, Rut Klinger, Sayaka Saitoh, Darran O'Connor, Yasuyuki Fujita, Dimitri Scholz, and

Nobue Itasaki. Dynamic and influential interaction of cancer cells with normal epithelial cells in 3D culture. *Cancer Cell International*, 14(1):1, 2014.

[10] Seher Balaban, Robert F Shearer, Lisa S Lee, Michelle van Geldermalsen, Mark Schreuder, Harrison C Shtein, Rose Cairns, Kristen C Thomas, Daniel J Fazakerley, Thomas Grewal, et al. Adipocyte lipolysis links obesity to breast cancer growth: adipocyte-derived fatty acids drive breast cancer cell proliferation and migration. *Cancer & Metabolism*, 5(1):1, 2017.

Chapter 4

Reconstructed segmental-long-spacing collagen *in vitro*

Another type of collagen-based biomaterial in this project is segmental-long-spacing (SLS) collagen, which shows a distinct block-like feature instead of the fibrillar structure of the typical aggregates of type I collagen, as shown in Figure 4.1. In each block of SLS collagen, the collagen monomers arrange laterally in register [1]. Other than being morphologically special, it also plays a significant role in studying the properties of the collagen monomer, which is normally difficult to study due to its small length scale (300 nm long, 1.5 nm in diameter [2]). In addition, SLS collagen has been identified in multiple tissues *in vivo*, such as human skin and cartilage [3]. Therefore, SLS collagen also possesses significance in biological systems.

Hence, there are practical applications to reconstructing SLS collagen *in vitro* in an easy and reproducible way. A former member of the Merschrod group, Chuan Xu, has reported one method to build SLS collagen in his thesis [4]. However, during my

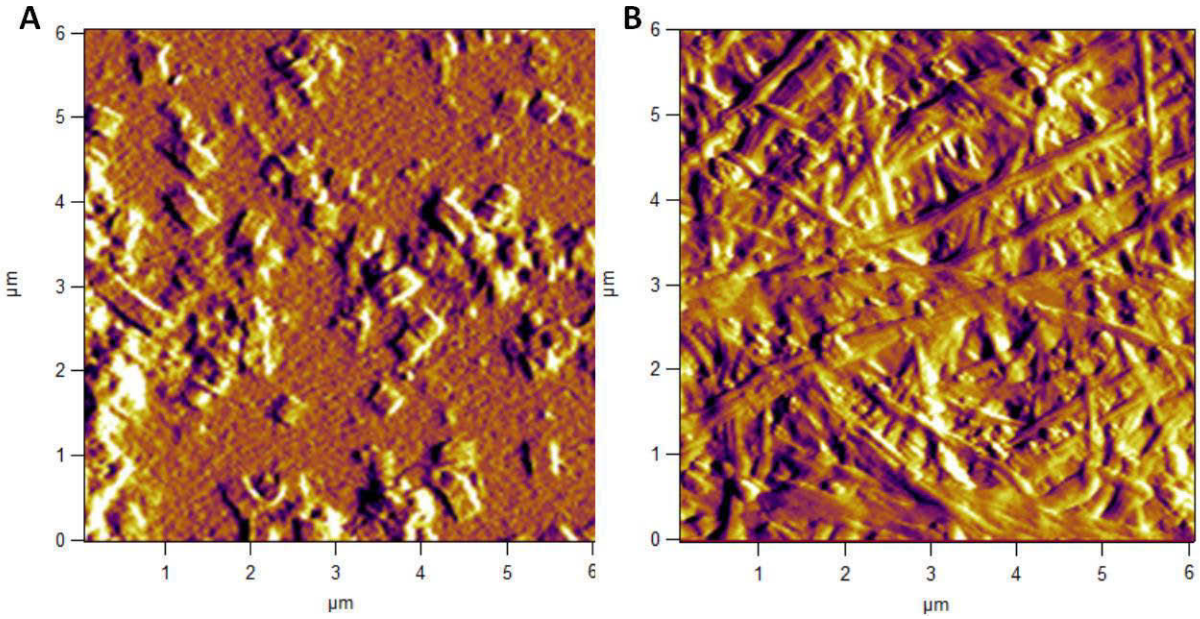

Figure 4.1: Two types of native type I collagen aggregations with very distinct morphologies, as seen in these deflection images. Image A: the SLS collagen shows the block-like structure. Image B: the regular fibrillar collagen structure.

scientific articles review, I developed a new way to synthesize SLS collagen, which has even better reproducibility. Herein I will present my method as well as some follow-up characterization conducted by using AFM. I also conducted research to investigate the influence of pH to the formation of SLS collagen. This is further to aim at discovering the specific mechanism of SLS collagen formation, which still remains poorly understood [5].

4.1 Experiment

The new method was developed from Xu's thesis [4] and Goh's work [6]. I used 156 μL of native type I collagen monomer solution (Advanced BioMatrix) with a concentration of 3.2 mg/mL, and diluted it with the addition of 446 μL of 0.05 % acetic acid. Then I dissolved 4 mg adenosine-5'-triphosphate (ATP) (Sigma) in 400 μL

of 0.05 % acetic acid. I mixed the two prepared solutions and adjusted the pH of the mixture to 2 or 4, to seek the influence of pH on SLS aggregations. The solutions sat at room temperature for roughly one hour, allowing the original transparent solutions to turn cloudy, which represents the formation of SLS collagen aggregates. Imaging required a ten-fold dilution air-dried on mica substrates.

The AFM scanning was performed in contact mode in air, using a MFP-3D AFM (Asylum Research, Santa Barbara, CA) and CSC37/CR-AU tips (Mikromasch, USA). The resonance frequency and spring constant of the tips were about 20 kHz and 0.3 N/m, respectively. The specific value was determined by the thermal noise method (Roger Proksch, Asylum Research).

4.2 Results and Discussion

4.2.1 Morphology

At lower pH (pH=2), as shown on Figure 4.2 A, numbers of tiny rectangular shaped blocks randomly distribute on the mica surface. To have a clearer view, I selected an area with sparse distribution of the blocks and zoomed in to obtain image B. On image B, a section analysis on individual blocks (not shown here) indicates that the length of each block is roughly 300 nm, which is the same as the length of one collagen monomer [7]. Therefore, the rectangular shaped blocks are assigned to be the formed SLS collagen aggregates. Consequently, the new method to synthesize SLS collagen is proven to be valid.

SLS prepared at higher pH (pH=4) shows very distinct morphology. Instead of forming block-like SLS collagen, the collagen monomers lined up to form long fibers, which were more similar to the normal type I collagen fibers, as shown in Figure 4.3 A. However, when zoomed in at any area, the block-like SLS collagen was actually

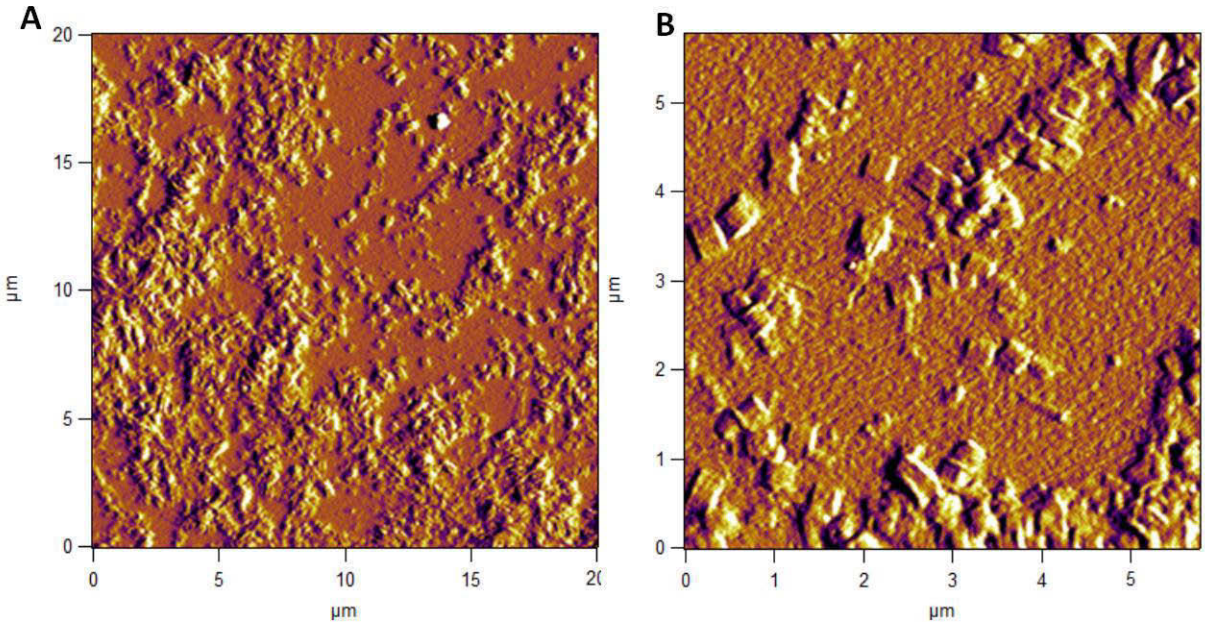

Figure 4.2: AFM images of SLS collagen samples with low pH (pH=2).

co-existing with the long fibers. The blocks show the tendency to line up one after another to form longer fibrillar structure, and the length of each block remains to be about 300 nm, hence the rising of pH did not denature or alter the geometry of the collagen monomers.

In summary, according to Figure 4.2 and Figure 4.3, with only slightly different pH value, the collagen monomers formed two very distinct structures. This finding implies pH plays a vital role in the formation of SLS collagen, with the more acidic environment favouring the complete formation of individual blocks.

4.2.2 Mechanics

I also studied the mechanics of SLS collagen by performing AFM minimum nano-indentation to evaluate if the addition of ATP molecules structurally modify the collagen monomers. Sixteen indentations distributed across an SLS collagen sample yielded the data used to extract Young's Moduli by fitting the obtained AFM

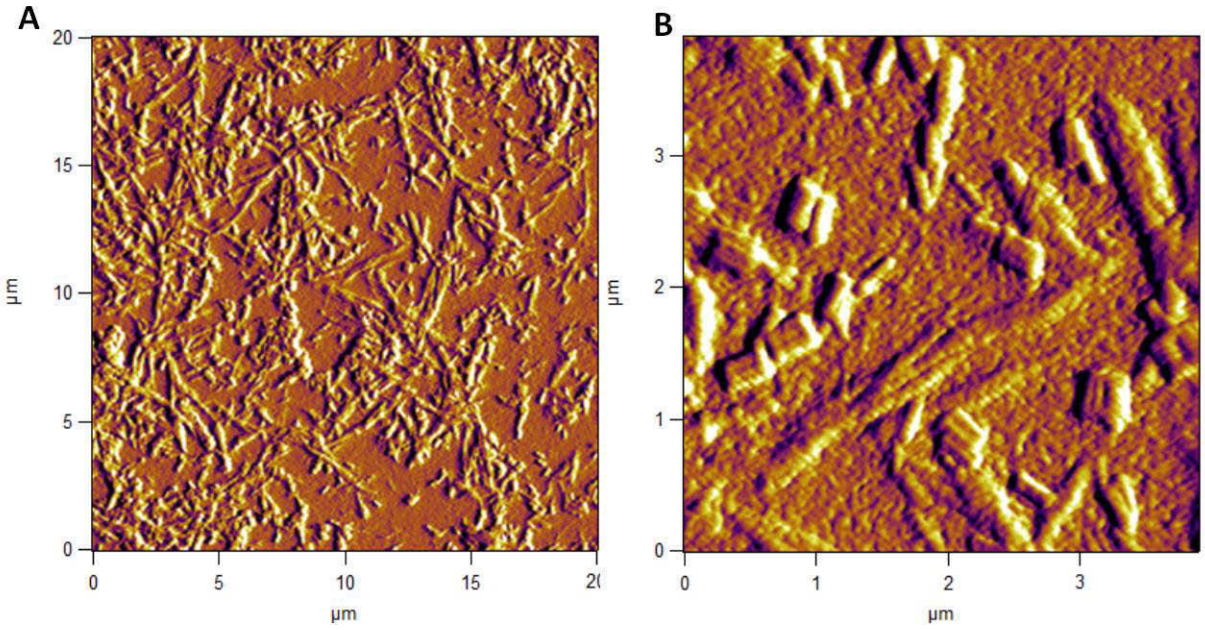

Figure 4.3: AFM images of SLS collagen samples with high pH (pH=4).

force curves with the JKR model. The resulting Young's modulus of SLS collagen is 2.690 ± 0.975 GPa, which is statistically indistinguishable from the measured Young's Modulus of the collagen sample without the addition of ATP molecules. Hence, my studies demonstrate that the different arrangement of collagen in SLS collagen aggregates does not lead to a mechanically distinct structure. The addition of ATP did not cause a change of the Young's Modulus of collagen, despite its purported role in linking monomers together. [5]

For further mechanical study, I focused on individual SLS collagen blocks, as in Figure 4.4. Multiple nano-indentations with a gradually increased indentation depth across the block served to check for plastic deformation. As indicated by Figure 4.4, there was no noticeable difference between the images before and after nano-indentation, even under a wide range of indentation depths. This demonstrates the elastic material nature of SLS collagen aggregates, that is to say their ability to restore their original shape after deformation.

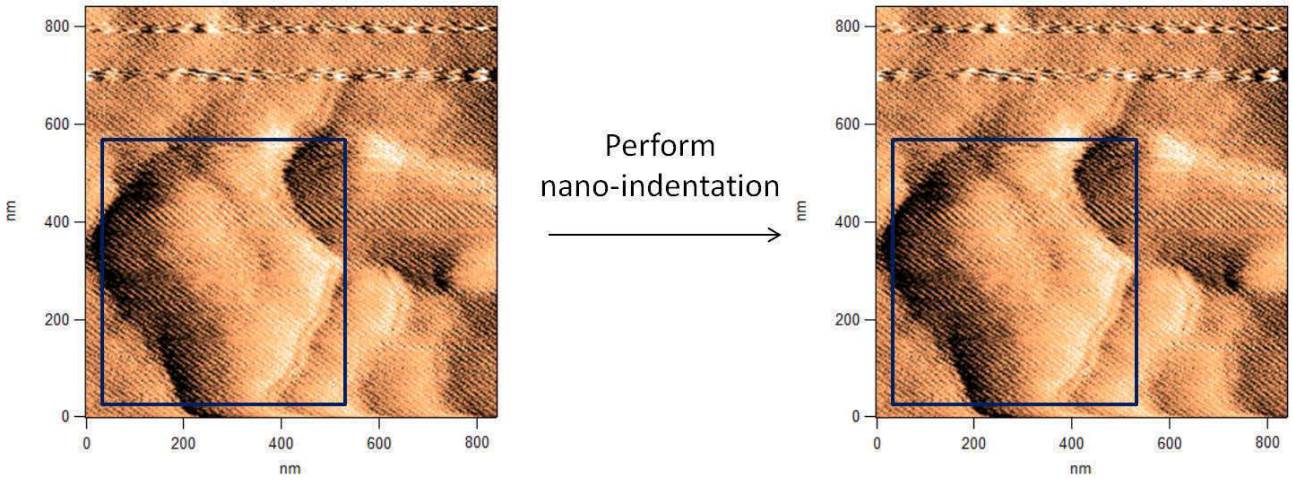

Figure 4.4: Indentations performed on individual SLS collagen aggregates did not cause irreversible deformation

4.3 Conclusions

In this chapter, I created and tested a new method of building SLS collagen *in vitro*, also studying the influence of pH with this synthesis protocol. Based on the AFM images, the less acidic environment (pH=4) contributes to the formation of long collagen fibrils, which is reminiscent of the natural structure of type I collagen aggregates. In contrast, the more acidic environment (pH=2) supports the formation of individual block-like SLS collagen, which is the aggregation of collagen monomers arranged in register. SLS collagen showed pure elastic (non-plastic) behaviour when responding to deformation over a wide range of indentation depths.

SLS collagen is one type of intriguing biomaterial, yet it has only very limited applications discovered by far. To date, the most common application of SLS is to study the properties of collagen monomers, as aforementioned. However, as revealed in this chapter, SLS collagen could be a tunable biomaterial under different synthesis environment. Even though I only studied the influence of pH, there are still many other factors, such as temperature and the concentration of ATP molecules, that can

be taken into consideration to tune the SLS collagen into various possible configurations. If future studies can elucidate the mechanism of SLS collagen formation, then potentially I can use it as a building block to construct long fibers, sheet-like structures etc. with the desired geometry to accommodate a number of applications ranging from designing matrices for cells to building bio-compatible artificial tissues.

Bibliography

[1] Yoshikazu Fujita, Kunihiko Kobayashi, and Takeshi Hoshino. Atomic force microscopy of collagen molecules. Surface morphology of segment–long–spacing (SLS) crystallites of collagen. *Journal of Electron Microscopy*, 46(4):321–326, 1997.

[2] Matthew D Shoulders and Ronald T Raines. Collagen structure and stability. *Annual Review of Biochemistry*, 78:929, 2009.

[3] Romaine R Bruns, DJ Hulmes, Stephen F Therrien, and Jerome Gross. Procollagen segment-long-spacing crystallites: their role in collagen fibrillogenesis. *Proceedings of the National Academy of Sciences*, 76(1):313–317, 1979.

[4] Chuan Xu. Nanostructure and Nanomechanics of Collagen Self-Assemblies. *PhD Thesis, Memorial University of Newfoundland*, 2014.

[5] J Robin Harris and Richard J Lewis. The collagen type I segment long spacing (SLS) and fibrillar forms: Formation by ATP and sulphonated diazo dyes. *Micron*, 86:36–47, 2016.

[6] MF Paige and MC Goh. Ultrastructure and assembly of segmental long spacing collagen studied by atomic force microscopy. *Micron*, 32(3):355–361, 2001.

[7] Ellen AG Chernoff and Donald A Chernoff. Atomic force microscope images of collagen fibers. *Journal of Vacuum Science & Technology A: Vacuum, Surfaces, and Films*, 10(4):596–599, 1992.

Chapter 5

Conclusions and future work

5.1 Conclusions

My research is focused on designing and investigating the properties of bio-compatible materials, which are mostly based on collagen. With the help of atomic force microscopy (AFM), a technique with high resolution and versatile applications, I successfully studied the morphology and mechanics of type I collagen matrices and segmental-long-spacing (SLS) collagen. This provided a preliminary understanding of the complicated interactions among adipocytes (fat cells), breast cancer cells, and the artificial matrices which I created.

By timing the addition of the type I collagen matrix, I firstly achieved selective manipulation of the release of leptin and adiponectin, which are reported to be the critical molecules that can regulate the behaviour of breast cancer cells [1, 2]. In addition to the therapeutic potential of this work, it also leads to my second project on co-culture of adipocytes and breast cancer cells on Matrigel, to investigate the detailed interactions between the target cells.

In the second project, I built a 3D co-culture system with adipocytes, the breast

cancer cells and a Matrigel matrix, in the collaboration with Dr. Sherri Christian (Department of /Biochemistry, Memorial University of Newfoundland). I present AFM images that confirm that the culture of adipocytes and breast cancer cells on Matrigel was achieved. As well, the shape change of breast cancer cells from spindle to spherical shape in the presence of adipocytes indicates the active interactions between the two types of cells in the system.

Till now, a few similar co-culture systems for adipocytes and breast cancer cells have been established by other research groups as well [3, 4]. However, they are more focused on the aspect of the biological interactions between the cells, such as the secretion of cytokines. In this thesis, other than analyzing the cytokines concentration, I also investigated to what extent the addition of the cells alter the mechanical properties of the cell matrices. The mechanics of the cell matrices play a vital role in regulating cell behaviour [5] that should not be neglected while evaluating the co-culture system. Hence in the future, there should be more research addressed regarding the mechanical properties of our artificial extracellular matrix (ECM).

Finally, I also modified the method of synthesizing segmental-long-spacing (SLS) collagen *in vitro* with an eye toward biomaterial applications. I found that pH played a vital role in the formation of SLS collagen and its superstructures. The more acidic ambience is in favour of forming individual SLS collagen blocks, while at a higher (though still acidic) pH one starts to see fibrous structures based on SLS components.

5.2 Future work

In the future, there is still much work to continue on, especially regarding the 3D co-cultural system as mentioned above. On the materials properties side, in this thesis, the elasticity of type I collagen matrices and the matrigel matrix has been thoroughly

investigated. However, visco-elasticity is another distinct character that biomaterials possess, and it always determines the functions of biological tissues [6]. Visco-elasticity is essentially a combination of viscosity and elasticity; it shows a variation of strain over time under a constant stress [7]. Despite the complexity of visco-elasticity, it can be conveniently measured by AFM [8] by applying a dwelling time on the AFM tip while conducting a nano-indentation. Hence, the next step will be focusing on the investigation of visco-elasticity of our artificial ECM. Considering the ill-defined composition of Matrigel, it would be best to start with better understood type I collagen matrices, which form part of the ECM in our system *in vivo*

Other than that, in the current system, I chose Matrigel as the artificial extracellular matrix (ECM), because it can offer cancer cells a more physiological environment, as well as serving as a common reconstituted basement membrane. However, the real ECM *in vivo* has both the interstitial matrix and the basement membrane as the major composition [9]. Hence, as the next step, I can consider incorporating type I collagen into the current artificial ECM and explore if that will change the interactions between cells.

pH is only one of many controllable experimental conditions in the formation of collagenous biomaterials. Others include solution temperature, the ATP molecule concentration, and the reaction time of the ATP and collagen monomer mixed solution. Starting from the diverse structures I achieved by only varying pH, these other parameters will like enable further tunable SLS collagen for various applications. For example, I do have the plan to incorporate the type I collagen into the 3D co-culture system, as introduced in Chapter 3. However, I am expecting some difficulties in that the uniform size of native type I collagen fibers cannot well accommodate both the adipocytes and the breast cancer cells, given the fact that they have very distinct geometry and cluster size [10, 11]. But, ideally, if I can build long fibers that con-

sist of SLS collagen blocks, I would be able to tune the fiber diameter and length corresponding to the physiological condition of the two types of cells.

Bibliography

[1] V. Dubois, T. Jarde, L. Delort, H. Billard, D. Bernard-Gallon, E. Berger, A. Geloen, M. P. Vasson, and F. Caldefie-Chezet. Leptin induces a proliferative response in breast cancer cells but not in normal breast cells. *Nutrition and Cancer*, 66(4):645–55, 2014.

[2] G. Li, L. Cong, J. Gasser, J. Zhao, K. Chen, and F. Li. Mechanisms underlying the anti-proliferative actions of adiponectin in human breast cancer cells, MCF7-dependency on the cAMP/protein kinase-A pathway. *Nutrition and Cancer*, 63(1):80–8, 2011.

[3] Manuel Picon-Ruiz, Chendong Pan, Katherine Drews-Elger, Kibeom Jang, Alexandra H Besser, Dekuang Zhao, Cynthia Morata-Tarifa, Minsoon Kim, Tan A Ince, Diana J Azzam, et al. Interactions between Adipocytes and Breast Cancer Cells Stimulate Cytokine Production and Drive Src/Sox2/miR-302b–Mediated Malignant Progression. *Cancer Research*, 76(2):491–504, 2016.

[4] Chen Wang, Chao Gao, Kui Meng, Haishi Qiao, and Yong Wang. Human adipocytes stimulate invasion of breast cancer MCF-7 cells by secreting IGFBP-2. *PloS One*, 10(3):e0119348, 2015.

[5] Brooke N Mason, Joseph P Califano, and Cynthia A Reinhart-King. Matrix stiffness: a regulator of cellular behavior and tissue formation. In *Engineering Biomaterials for Regenerative Medicine*, pages 19–37. Springer, 2012.

[6] Juan de Vicente. *Viscoelasticity: From Theory to Biological Applications*. InTech, 2012.

[7] Richard Christensen. *Theory of viscoelasticity: an introduction*. Elsevier, 2012.

[8] AC Fischer-Cripps. A simple phenomenological approach to nanoindentation creep. *Materials Science and Engineering: A*, 385(1):74–82, 2004.

[9] Bruce Alberts, Alexander Johnson, Julian Lewis, Martin Raff, Keith Roberts, and Peter Walter. The extracellular matrix of animals. 2002.

[10] C Farnier, S Krief, M Blache, F Diot-Dupuy, G Mory, P Ferre, and R Bazin. Adipocyte functions are modulated by cell size change: potential involvement of an integrin/ERK signalling pathway. *International Journal of Obesity*, 27(10):1178–1186, 2003.

[11] A Fatih Sarioglu, Nicola Aceto, Nikola Kojic, Maria C Donaldson, Mahnaz Zeinali, Bashar Hamza, Amanda Engstrom, Huili Zhu, Tilak K Sundaresan, David T Miyamoto, et al. A microfluidic device for label-free, physical capture of circulating tumor cell clusters. *Nature Methods*, 12(7):685–691, 2015.

Appendix A

Attaching a spherical tip to the tipless AFM cantilever

The sharpness of AFM tips brings AFM with high resolution; however, it also limits the application of AFM, especially for the force spectroscopy. Biological samples usually give different mechanical response when measured under different length scales. Therefore, it would be logical to perform indentation to access the mechanics of samples by using tips ranging from different length scales.

To achieve this, I attached a silica micro-bead with 30 µm radius to a tipless AFM cantilever, as outlined below.

1. Dilute the silica microbead solution. The specific concentration depends on sphere size, charging of surface groups (i.e. suspension medium pH and ionic strength), tip coating, tip shape, and many other effects; this is best determined in an ad-hoc fashion. (See next step.)

2. Deposit diluted solution on a glass slide. Observe through the microscope on the AFM to check for individual silica microbeads, as shown in Figure A.1A, instead of the microbead clusters. (If not, repeat Step 1)

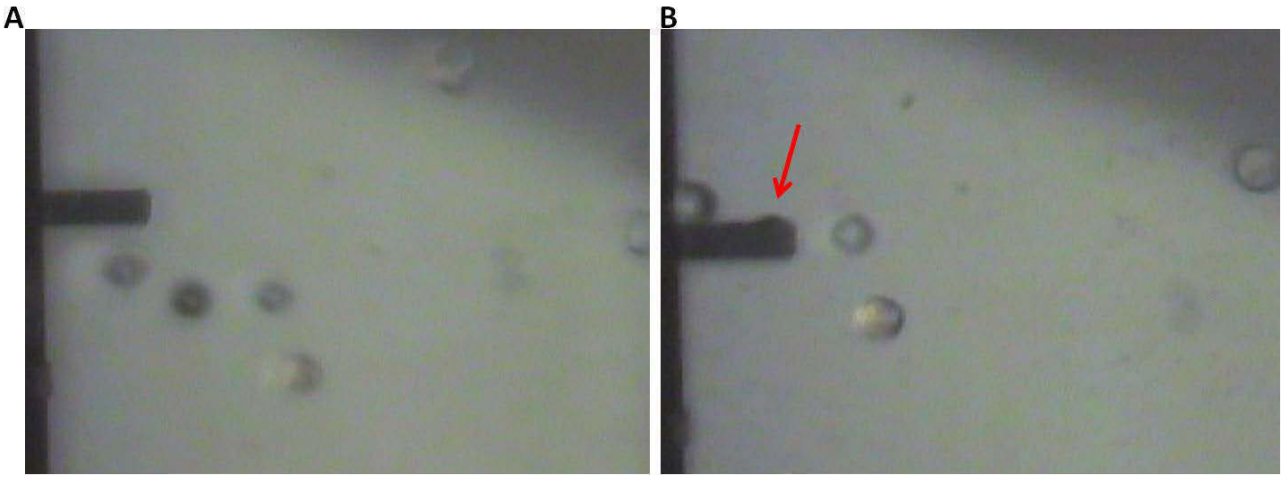

Figure A.1: The process of attaching spherical tip to tipless AFM cantilever. A: individual silica microbeads. B: one sphere attached to an AFM probe cantilever; the arrow indicates the edge of the sphere

3. Deposit glue on the glass slide, then using the probe or sample stage micrometers for the AFM position the cantilever above the glue and perform an indentation to make sure that there is glue on the end of the cantilever.

4. Position the cantilever above the individual microbead, then performe another indentation. Raise the cantilever with attached sphere as shown in Figure A.1B

5. Leave the attached cantilever to air-dry for an hour.

I took a SEM micrograph to ensure that the sphere is attached in place. The SEM image is shown in Figure A.2

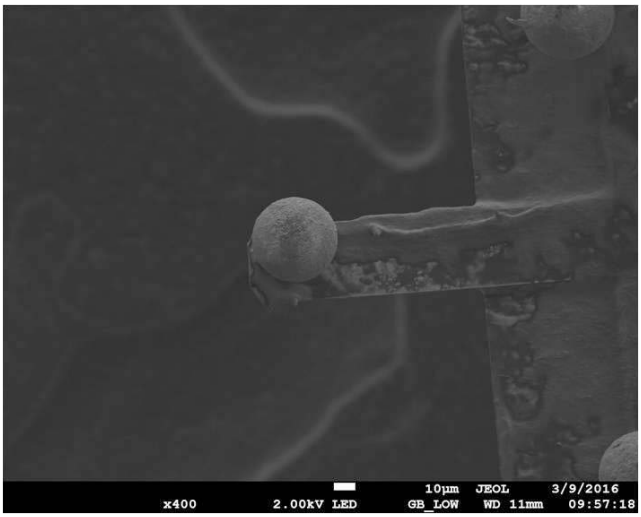

Figure A.2: SEM image of AFM cantilever with a sphere attached.

Appendix B

A introduction to the Bligh-Dyer method

In Chapter 2, to determine the triglyceride accumulation, the Bligh-Dyer method was employed to extract lipids from the resuspended cells. The Bligh-Dyer method is a well-established technique to efficiently extract and purify lipids from biological materials. [1]

Here are the procedures of carrying out the Bligh-Dyer method.

1. Homogenize the biological tissue with chloroform and methanol.
2. Add water and chloroform to dilute and separate the formed solution into two layers.
3. Separate the chloroform layer, which comprises the targeting lipids.

In this thesis, the obtained lipids were re-extracted and purified as described below, to increase the accuracy of the triglyceride accumulation measurement. Following the removal of the organic solvent layer from the Bligh-Dyer extraction, lipids remaining in the upper phase were re-extracted (in duplicate) by adding 2.5 mL of chloroform,

vortexing for 30 s, and centrifuging at 1000 ×g for 5 min. The organic solvent layer was removed and pooled with the organic solvent layer from the Bligh-Dyer extraction. The pooled extracts were back-extracted by mixing with an equal volume of PBS, vortexing for 30 s, and centrifuging at 1000 ×g for 5 min. The organic solvent layer was removed, dried under N_2(g), resuspended in 500 μL isopropanol, and stored under N_2(g) at –20 °C until needed.

To control for extraction efficiency, 10 μg of a triacylglycerol (TG) standard (cat. no. 17810, Sigma Aldrich, St. Louis, MO, USA) was extracted as above, and the TG quantified with 25 μL of extracted sample (n=11) was compared to the TG quantified from 25 μL of 0.02 μg/μL TG standard (in isopropanol). TG cellular accumulation was corrected for extraction efficiencies within each extraction procedure (mean extraction efficiency was 88.2% with a range of 79.8%-97.7%.) A colorimetric commercial kit from Wako Diagnostics (Richmond, VA, USA) was used to quantify TG, using standard curve of 0-50 μg TG.

Bibliography

[1] E Graham Bligh and W Justin Dyer. A rapid method of total lipid extraction and purification. *Canadian Journal of Biochemistry and Physiology*, 37(8):911–917, 1959.

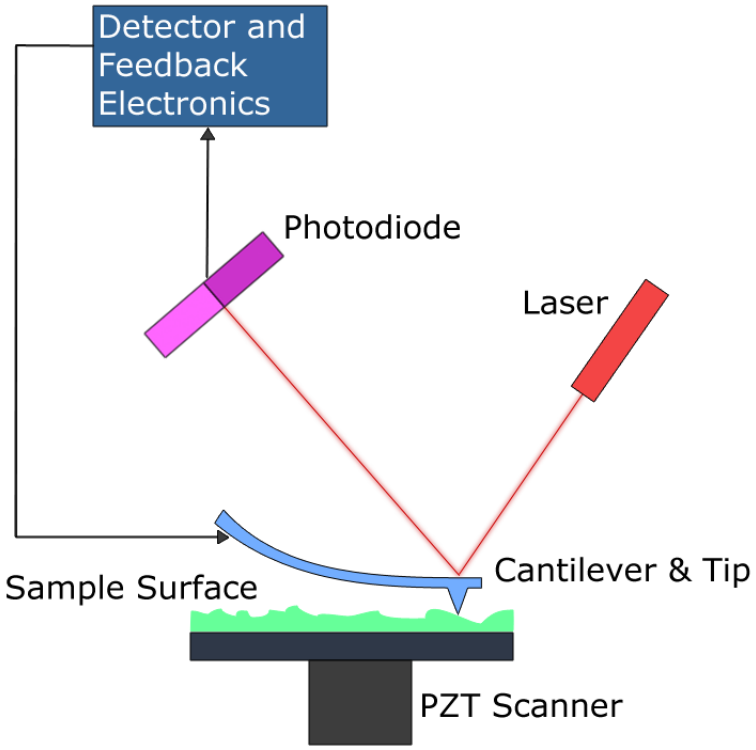

Figure 1.6: The schematic of the AFM setup. By Askewmind [Public domain], via Wikimedia Commons

being damaged. In my project, most of the study was done under contact mode.

In contact mode, the AFM tip keeps in contact with the sample surface during scanning. So once the tip meets higher or lower features, the cantilever will correspondingly bend against or towards the sample to make sure the tip and sample are in contact. This bending causes a variation in deflection of the laser. Then a feedback loop adjusts the deflection back to a pre-defined "setpoint". In tapping mode, however, instead of remaining in contact with sample, the AFM tip keeps tapping on the sample surface with a set amplitude and frequency. The surface features cause a change of tapping amplitude, which is recorded and adjusted back to the setpoint by the feedback loop. [48]